# REPORT DOCUMENTATION PAGE

AFRL-SR-AR-TR-03-0214



| 1. REPORT DATE (DD-MM-YYYY) | 2. REPORT TYPE | 3. DATES COVERED (From - To) |
|---|---|---|
| 04-06-2003 | Final Technical Report | 01-05-2000 to 30-11-2002 |

**4. TITLE AND SUBTITLE**
Fuels Combustion Research: Supercritical Fuel Pyrolysis

**5a. CONTRACT NUMBER**

**5b. GRANT NUMBER**
F49620-00-1-0298

**5c. PROGRAM ELEMENT NUMBER**
61102F

**6. AUTHOR(S)**
Mary J. Wornat, Elmer B. Ledesma, Philip G. Felton, Joseph A. Sivo, Nathan D. Marsh

**5d. PROJECT NUMBER**
2308

**5e. TASK NUMBER**
BX

**5f. WORK UNIT NUMBER**

**7. PERFORMING ORGANIZATION NAME(S) AND ADDRESS(ES)**
Princeton University
Department of Mechanical and Aerospace Engineering
Engineering Quadrangle, Olden Street
Princeton, New Jersey 08544-5263

**8. PERFORMING ORGANIZATION REPORT NUMBER**

**9. SPONSORING/MONITORING AGENCY NAME(S) AND ADDRESS(ES)**
AFOSR/NA
4015 Wilson Boulevard
Room 713
Arlington, Virginia 22203

**10. SPONSOR/MONITOR'S ACRONYM(S)**

**11. SPONSOR/MONITOR'S REPORT NUMBER(S)**

**12. DISTRIBUTION/AVAILABILITY STATEMENT**
Approved for public release; distribution unlimited

20030623 008

**13. SUPPLEMENTARY NOTES**

**14. ABSTRACT**

Supercritical pyrolysis experiments were conducted with toluene, methylcyclohexane, and n-heptane at temperatures up to 585 C, pressures up to 100 atm, and residence times up to 550 sec. Analysis, by HPLC/UV, of the toluene reaction products led to the unequivocal identification of 27 individual PAH, up to 10 rings in size. The experiments showed that PAH yields increased exponentially with pressure. For each of the product PAH, values of the preexponential factor A and the activation volume V* were determined for the pressure-dependent global first-order kinetic rate constant. PAH yields were also extremely sensitive to temperature. At 100 atm and 480 C, PAH of only up to 2 rings were observed; at 535 C, PAH up to 10 rings were formed; at 585 C, solid deposits formed, plugging the reactor. Similar pressure and temperature sensitivities were exhibited by the PAH produced by methylcyclohexane. The nature of the PAH product distributions suggested that condensation reactions, involving the addition of aromatic structures and hydrogen loss, were a dominant mechanism for PAH formation in the supercritical environment.

**15. SUBJECT TERMS**
supercritical hydrocarbon pyrolysis, polycyclic aromatic hydrocarbons, endothermic fuels, fuel-line deposits, hypersonic aircraft fuels, reaction kinetics, PAH formation, pressure effects

| 16. SECURITY CLASSIFICATION OF: | | | 17. LIMITATION OF ABSTRACT | 18. NUMBER OF PAGES | 19a. NAME OF RESPONSIBLE PERSON |
|---|---|---|---|---|---|
| a. REPORT | b. ABSTRACT | c. THIS PAGE | | | Julian M. Tishkoff |
| Unclassified | Unclassified | Unclassified | UL | 66 | 19b. TELEPHONE NUMBER (Include area code) (703) 696-8478 |

6/19/03

FUELS COMBUSTION RESEARCH: SUPERCRITICAL FUEL PYROLYSIS

## Table of Contents

## Background and Introduction

The fuels used in the next generation of hypersonic aircraft will have to operate under very high pressures and will have to sustain very high heat loads (*e.g.*, 30,000 BTU/min) [1,2]) in order to meet aircraft cooling requirements. Within the fuel lines and injection system, where residence times can be many minutes, fuel temperatures and pressures may reach or exceed 540 °C (813 K) and 150 atm [2]—temperatures and pressures that exceed the critical temperatures and pressures of most pure hydrocarbons and jet fuels such as JP-7 and JP-8 [3]. At these temperatures and pressures, the fuel can undergo pyrolytic reactions, which have the potential of forming solid deposits that can clog fuel lines, foul fuel nozzles, and lead to undesirable or even disastrous effects for the aircraft.

The current inability to predict solids formation tendencies of fuels under supercritical conditions has been brought to our attention by Dr. Tim Edwards (Fuels Section, AFRL Turbine Engine Division, Wright-Patterson Air Force Base, Ohio), who shared with us solid deposition results for various jet fuels and *n*-octane, from scramjet test rigs at United Technologies Research Center (UTRC) [4]. The tests show that the tendency to produce solid deposits increases in the order: JP-7 < RP-1 < JP-8+100 < JP-10 < *n*-octane—an order that would not have been predicted, based solely on the proportions of paraffins, naphthenes, and aromatics in the fuels. Clearly we need to know more about the pyrolysis reactions of these fuels under supercritical conditions. In order to develop reliable fuel systems for high-speed aircraft that will not be subject to solid deposit formation, we need a thorough understanding of the pyrolysis behavior of candidate fuels under the supercritical conditions that they will be operating. Of particular interest are the reactions leading to polycyclic aromatic hydrocarbons (PAH), which serve as precursors to fuel-line deposits.

The fact that the fuel pyrolysis environment is a supercritical one introduces several complexities. With regard to physical properties, supercritical fluids have highly variable densities, no surface tension, and transport properties (*i.e.*, mass, energy, and momentum diffusivities) comparable to those of gases. Solvent-solute interactions, absent in the gas phase,

can exhibit huge effects in supercritical fluids, often affecting chemical reaction pathways by facilitating the formation of certain transition states [5]. Because solvent-solute interactions are very dependent on pressure, chemical reaction rates in supercritical fluids can be highly pressure-dependent [5-8]. The kinetic reaction rate constant k has been shown [6,9] to vary exponentially with pressure, according to the expression

$$k = A \exp[(-\Delta V^*/RT)p]$$

where $A$ is the preexponential factor (in $sec^{-1}$) and $\Delta V^*$ is the activation volume (in L/mole). As the equation shows, a negative value of $\Delta V^*$ denotes that the reaction is favored by an increase in pressure. The magnitude of $\Delta V^*$ is an index of how sensitive the reaction rate is to pressure. For gases, $\Delta V^*$ is essentially zero; for liquids, $\Delta V^*$ is on the order of $10^{-2}$ L/mole; for supercritical fluids, $\Delta V^*$ is on the order of 1 to 10 L/mole [9].

For the case of fuel pyrolysis reactions, Stewart *et al.* [10-12] have demonstrated that reaction pathways and reaction kinetics indeed differ between the gas phase and the supercritical phase. Their pyrolysis experiments with decalin and methylcyclohexane in an atmospheric-pressure flow reactor and in the very supercritical pyrolysis reactor currently in our use show that under supercritical conditions—but not in the gas phase at atmospheric pressure—both decalin and methylcyclohexane are able to produce methylated $C_5$-ring intermediates that readily convert to structures containing 6-membered aromatic rings. These aromatic rings can then serve as kernels for further cyclic growth to PAH and ultimately solid deposits. For the same two fuels, decalin and methylcyclohexane, Stewart *et al.* [10-12] also report different global Arrhenius kinetic rate parameters A and $E_a$ for their supercritical pyrolysis experiments, compared to their gas-phase experiments. We thus see that reaction pathways and reaction kinetics in the supercritical phase are substantially different from those in the gas or liquid phase. Therefore even for fuels whose gas-phase or liquid-phase pyrolysis behavior is well understood, it is of critical importance to study their pyrolysis in the supercritical phase, if these fuels are to be considered for future high-speed aircraft.

To that end, we have begun an experimental research program on the supercritical pyrolysis of model fuels. The model fuels include both aromatic and aliphatic components of jet fuels, as well as methylcyclohexane, an "endothermic" fuel which has attracted interest due to its high heat-absorbing capacity as it would undergo endothermic dehydrogenation prior to combustion. We have chosen these well-defined model fuels rather than an actual multicomponent jet fuel like JP-7 or JP-8, so that we can trace reaction pathways from starting material to PAH to solid deposits—with the aim of gaining an understanding of the fundamental reaction processes taking place. Knowledge of individual components' behavior lays the fundamental groundwork for later examining these components in combination with one another, leading to the eventual understanding of what takes place with fuels that are more complex mixtures. What we learn of the pyrolysis behavior of certain components should provide crucial information for the assessment of solid-deposit formation tendencies in existing fuels and for the formulation of new fuels that may be more resistant to solid deposit formation.

Our supercritical pyrolysis experiments [14,15] make use of the reactor designed by Davis [13] and used by Stewart *et al.* [10,12] for earlier supercritical pyrolysis experiments with model fuels. Since the main focus of our work is the formation of fuel-line deposits during supercritical pyrolysis and since PAH are precursors to fuel-line deposits, a critical component of our work is the chemical analysis of large PAH, for which we employ high-pressure liquid chromatography (HPLC) with diode-array ultraviolet-visible (UV) absorption detection, a technique ideally suited for isomer-specific PAH analysis.

In the following, we first describe the experimental equipment and techniques used in the supercritical pyrolysis experiments. We report the results of our experiments with toluene, *n*-heptane, and methylcyclohexane—delineating the regimes of PAH and solid-deposit formation, discussing the effects of temperature and pressure on PAH product yields, reporting values of global kinetic rate parameters for individual PAH, and presenting overall PAH-formation reaction pathways consistent with our experimental observations. We then summarize the key results and present recommendations for future work.

## Experimental Equipment and Techniques

*Reactor System*

The supercritical fuel pyrolysis experiments have been conducted in an isothermal, isobaric reactor designed expressly for such experiments by Davis [13] and used by Stewart [10,12] in an AFOSR-sponsored research program supervised by Professor Irvin Glassman at Princeton University. Upon his retirement, Professor Glassman made the reactor available to us for continuing supercritical fuels pyrolysis research.

The reactor system is illustrated in Figure 1. Prior to an experiment, the liquid fuel (99.9+% pure) is sparged with nitrogen for three hours, as described by Stewart [10], to get rid of any dissolved oxygen that could introduce auto-oxidative effects [16]. The sparged fuel is then loaded into a high-pressure nonreciprocating pump, which delivers the fuel to the reactor, as shown in Figure 1. The reactor itself is a coil of 1-mm i.d., 1.59-mm o.d. capillary tube made of silica-lined stainless steel. (The silica lining prevents wall-catalyzed deposit formation that occurs with unlined stainless steel [10,13,17].) The reactor coil is immersed in a temperature-controlled fluidized-alumina bath, which ensures isothermality throughout the reactor length. As indicated in Figure 1, the entrance and exit lines of the reactor are passed through a water-cooled heat exchanger to ensure a controlled thermal history and residence time. Exiting the heat exchanger, the quenched reaction products pass through a stainless steel filter (hole size, 5 μm) and on to a six-position high-pressure valve, for product collection. A dome-loaded back-pressure regulator, downstream of the valve, controls the system pressure, to within $\pm$0.2 atm, up to a maximum of 110 atm. A burst disk, located upstream of the reactor, provides a safe flow outlet, in case of over-pressurization.

Reactor residence time is varied by changing the length of the reactor coil. The reactor system is capable of operating at temperatures up to 860 K, pressures up to 110 atm, and residence times up to 3600 sec—operating ranges relevant to those envisioned for fuel systems in future hypersonic aircraft [2]. As documented by Davis [13] and Stewart [10], the reactor has been designed to meet Cutler's [18] and Lee's [19] criteria for idealization as plug flow, with regard to

species concentration profiles. The resulting radially uniform species concentrations, coupled with the reactor's constant-temperature and constant-pressure operation, render this reactor ideal for supercritical pyrolysis kinetics experiments.

Pyrolysis experiments have been performed with the following model fuels: *n*-heptane (critical temperature, 267 °C; critical pressure, 27 atm), an aliphatic component of jet fuels; methylcyclohexane (critical temperature, 299 °C; critical pressure, 34 atm), a model fuel of interest to the Air Force due to its high heat-absorbing capacity as it would undergo an endothermic dehydrogenation reaction in the fuel lines, prior to combustion; and toluene (critical temperature, 319 °C; critical pressure, 41 atm), an aromatic component of jet fuels as well as the dehydrogenation product of the endothermic fuel methylcyclohexane.

*Product Analysis*

At the conclusion of a pyrolysis experiment, the liquid-phase reaction products are removed from the high-pressure collection valve and transferred to a vial. Two separate 10-μL aliquots of the product solution are removed for injection onto the gas chromatograph, which analyzes the smaller aromatic products (1 to 4 rings). The remainder of the product solution (~1 mL) is prepared for high-pressure liquid chromatography (HPLC), which analyzes the larger aromatic products ($\geq$ 3 rings).

Gas chromatographic analysis of the supercritical fuel pyrolysis products is performed on an Agilent Model 6890 gas chromatograph (GC) with flame-ionization detector (FID), in conjunction with an Agilent Model 5973 mass spectrometer (MS). A sample volume of 10 μL is injected by syringe, through a split injector, onto an HP-5 fused silica capillary column of length, 30 m; diameter, 0.25 mm; and film thickness, 0.1 μm. The column temperature is programmed to hold at 40 °C for the first 3 minutes; it is then ramped at 4 °C /min to 300 °C, where it is held for 15 minutes. The GC/FID/MS instrument is used to quantify 1- to 4-ring aromatic products—all of which are identified by matching retention times and mass spectra with those of reference standards.

The portion of the product solution reserved for HPLC analysis is concentrated in a Kuderna-Danish apparatus and exchanged, under nitrogen, into 100 μL of dimethylsulfoxide, a solvent compatible with the solvents used in the HPLC method employed for PAH analysis. During the concentration and solvent-exchange procedure, portions of the more volatile aromatics such as the 1- and 2-ring species, are lost to vaporization; hence these lighter aromatic products are quantified by gas chromatographic analysis, as described above.

For analysis of the large aromatic products ($\geq$ 3 rings) by HPLC, a 20-μL aliquot of the product/dimethylsulfoxide solution is injected onto a Hewlett-Packard Model 1050 high-pressure liquid chromatograph, coupled to a diode-array ultraviolet-visible (UV) absorbance detector. The chromatographic separation method [20,21], optimized for large PAH analysis, utilizes a reversed-phase Vydac 201-TP octadecylsilica column of particle size, 5 μm; inner diameter, 4.6 mm; and length, 250 mm. A time-programmed sequence of solvents—acetonitrile/water, acetonitrile, and dichloromethane—is pumped through the column, and the PAH product components elute in the order of increasing molecular size. UV absorbance spectra are taken, every 0.6 seconds, of the exiting components, which are then identified by matching the UV absorbance spectra (and elution times) with those of commercially available and specially synthesized reference standards. Quantification of each species is based on extensive calibration with reference standards, over a broad range of concentrations.

HPLC/UV is particularly well suited for analyzing the large PAH molecules that are precursors to fuel-line solid deposits for two reasons: 1) Large PAH are too involatile to be analyzed by gas chromatography but are amenable to analysis by HPLC. 2) For large PAH there are many different isomeric structures possible for a given $C_xH_y$ formula. (For example, there are 65 possible isomers of 6-ring PAH of formula $C_{24}H_{14}$ [22].) The product identification method, therefore, must be able to unequivocally distinguish between different PAH isomers. HPLC/UV permits this unequivocal identification of PAH, since the identification is made by matching each product component's unique UV absorbance spectrum with that of a reference standard. Through the years, the principal investigator has amassed a library of hundreds of UV spectra of PAH,

many of which have been obtained from specially synthesized reference standards, expressly for this purpose. In previous pyrolysis and combustion studies, the principal investigator has successfully employed HPLC/UV to analyze complex mixtures of product PAH from fuels such as coal [23-26], anthracene [20,21,27], benzene [28], and catechol [29]. It should be emphasized that the HPLC/UV means of analyzing large PAH is a very highly specialized technique—a capability of only a few laboratories in the world.

## Research Results and Discussion

*Pyrolysis of Toluene: PAH Products Identified*

Pyrolysis experiments have been conducted with toluene at temperatures up to 585 °C, pressures up to 100 atm, and residence times up to 550 sec. Over the ranges of conditions investigated, the highest-yield aromatic products from our supercritical toluene pyrolysis experiments are benzene, the three xylenes, and the ten bi-toluyls. Figure 2 presents the yields of these major products, measured by GC/FID/MS, as functions of pressure, for experiments run at 535 °C and 550 sec. All of these products are observed in gas-phase toluene pyrolysis experiments [30] and result from straight-forward reaction steps. Displacement of toluene's methyl group by H gives benzene. Displacement of any of toluene's aryl hydrogens by methyl gives the xylenes. The various bi-toluyls arise from abstraction of H from toluene (at any of various sites) to form a radical, which then displaces an H (at any of various sites) on another toluene molecule. Activation energies [30] for the various types of bond-breaking steps in these reactions are shown in Figure 3. It is important to note that to form any of the reaction products in Figure 2 requires breaking of only single bonds, either C-H or C-C, and does not involve the breaking of the aromatic ring in toluene's structure.

Figure 4 presents an HPLC chromatogram of the products of supercritical toluene pyrolysis at 535 °C, 550 sec, and 100 atm, the highest pressure in Figure 2. Depicted in Figure 4 are the structures of the twenty-seven 2- to 10-ring PAH that have been unequivocally identified by HPLC/UV in this product mixture. (The cluster of large peaks in the 12- to 20-minute retention time range corresponds to the bi-toluyls, which are better resolved by GC and thus not individually

labelled with product structures in Figure 4. PAH such as phenanthrene and anthracene, which elute on the HPLC in the same time range as the bi-toluyls, are quantified by GC instead of HPLC, to avoid signal interference.) Most of the 2- to 5-ring PAH in Figure 4 have been identified by others [30,31] as products of toluene pyrolysis at subcritical pressures. Those studies, however, do not report PAH of > 5 rings, such as the nine 6- to 10-ring PAH found in the supercritical pyrolysis products of Figure 4.

Of particular note in Figure 4 are the four very large PAH of 8, 9, and 10 fused aromatic rings—benzo[*a*]coronene, benzo[*pqr*]naphtho[8,1,2-*bcd*]perylene, naphtho[8,1,2-*abc*]coronene, and ovalene—none of which have ever before been identified as products of toluene pyrolysis or as products of supercritical pyrolysis of any fuel. The UV spectral matches confirming the identifications of these 8- to 10-ring PAH, as well as the 6- and 7-ring PAH, are displayed in Figures 5-8. It should be noted that it is rare for any of the 8- to 10-ring PAH to be observed in fuel products—partly because few researchers have the analytical techniques or the specially synthesized reference standards [32] necessary to identify these species and partly because formation of these large PAH requires extreme conditions. For example, one of the only other cases in which the large PAH ovalene has been shown [33] to be produced is from subcritical fuel-rich combustion of naphthalene/ethylene mixtures at 1375 °C (840 °C hotter than the temperature in Figure 4). The fact that the monocyclic fuel toluene can produce the 10-ring ovalene at a temperature of only 535 °C points to the huge effect of the supercritical pressure conditions in facilitating the formation of large PAH, which can be precursors to solid deposits.

*Temperature Effects and Solid Deposits Formation*

That these large PAH are precursors to solid deposits is corroborated by the fact that our supercritical toluene pyrolysis experiments at 100 atm and 585 °C (just 50 °C higher than the temperature corresponding to Figure 4) result in repeated plugging of the reactor, due to solid deposit formation. This extreme sensitivity to temperature, in the high-pressure supercritical pyrolysis environment, is further illustrated by comparison of Figure 4, the chromatogram of toluene products at 100 atm and 535 °C, with Figure 9, the chromatogram of toluene products at

100 atm and 480 °C. Figure 9 shows that at 480 °C, just 55 °C lower than the temperature in Figure 4, no PAH of greater than 2 aromatic rings are detected. In addition, the bi-toluyls formed at 480 °C are a factor of 20 smaller in yield than those formed at 535 °C. We thus see that at supercritical pressures, the formation of bi-toluyls, PAH, and solid deposits are all extremely sensitive to temperature: At 100 atm, within a hundred-°C span of temperature, there is transition from a regime in which only bi-toluyls and small PAH are produced, to one in which large PAH are produced (and smaller ones in more abundance), and then to a regime in which solid deposits are produced.

*Pressure Effects*

The results from the supercritical toluene pyrolysis experiments show that in addition to being very sensitive to temperature, PAH formation in a supercritical pyrolysis environment is also very sensitive to pressure. Figures 10-23 present the yields, as functions of pressure, of the 2- to 10-ring PAH produced by toluene pyrolysis at 535 °C. As demonstrated in these figures, yields of all the PAH increase continuously with pressure, rising particularly dramatically at pressures above the toluene critical pressure of 41 atm.

Figure 15 reveals a result peculiar to high-pressure toluene pyrolysis. Unlike results observed for toluene at atmospheric pressure [31], Figure 15 reveals that in the supercritical toluene experiments, yields of anthracene exceed those of its $C_{14}H_{10}$ isomer phenanthrene. A similar finding is reported [30] for toluene pyrolysis at 10 atm. Both of these $C_{14}H_{10}$ PAH, anthracene and phenanthrene, can result from the combination of toluene and benzyl radical, as illustrated in Figure 24 (adopted and extended from Colket and Seery [30]). The observed dominance of anthracene over phenanthrene suggests that at high pressures, union of the benzyl radical to an aryl site of toluene (top pathway of Figure 24) is preferred over union at the benzyllic site (bottom pathway). This observation on the relative yields of the $C_{14}H_{10}$ PAH illustrates the importance of pressure in determining reaction pathway. The dominance of pyrene over its $C_{16}H_{10}$ isomer fluoranthene, in Figure 16, and the dominance of benzo[*ghi*]perylene over its $C_{22}H_{12}$ isomer indeno[1,2,3-*cd*]pyrene, in Figure 20, are also results peculiar to this high-pressure environment

and contrary to observations in atmospheric-pressure pyrolysis systems [20,26,28,29]. These differences in relative abundances within isomer families suggest that the mechanisms for PAH formation in the high-pressure environment differ from those in the atmospheric-pressure environments.

*PAH Formation Mechanisms*

Figure 24 shows how anthracene and phenanthrene can be formed from supercritical toluene pyrolysis, but the question arises as to how others of the toluene product PAH in Figure 4 can be formed. Most of the literature on PAH formation from fuels combustion and pyrolysis invokes some version of the $C_2$-addition mechanism [34,35], in which sequential addition of 2-carbon hydrocarbons such as ethylene, acetylene, or their radicals leads to aromatic structures of successively larger ring number. This mechanism, widely applicable in high-temperature, subcritical pyrolysis environments, does not, however, apply to our supercritical toluene pyrolysis environment in which temperature is much lower, acetylene is not formed, toluene conversion is very low, and product selectivity is high (*i.e.*, for a given number of rings, only certain species are found, out of large numbers of possibilities.). The absence, from Figures 4 and 9, of $C_2$-addition products—such as the cyclopenta-fused PAH and ethynyl-substituted PAH in Figure 25, which we routinely see in high-temperature, atmospheric-pressure pyrolysis of a variety of fuels [23,27,29,36-39]—confirms that the $C_2$-addition mechanism is not active under the conditions of our supercritical toluene pyrolysis experiments.

In the lower-temperature, high-pressure reaction environment of our supercritical pyrolysis experiments, in which there is no evidence of aromatic ring rupture, it would be logical that the larger PAH would be produced from combination of the aromatic building blocks available. Figure 24 illustrates how two of the product PAH in Figure 4 can be formed by combination of toluene and its most readily formed radical, benzyl. Although toluene is the most plentiful species in our reaction environment, other aromatic building blocks are available: the major products from Figure 2—benzene, the xylenes, and the bi-toluyls—as well as the product PAH themselves. Figure 26 shows how three of the products of Figure 4—pyrene, coronene, and ovalene—can be

formed by combinations of the xylenes and their radicals. Subsequent methyl displacement of an aryl hydrogen on either pyrene or coronene would lead to the 1-methylpyrene or 1-methylcoronene in Figure 4.

Figures 27-29 illustrate postulated schemes for the formation of other large PAH observed in Figure 4: the 8-ring benzo[*pqr*]naphtho[8,1,2-*bcd*]perylene (Figure 27), the 6-ring benzo[*ghi*]perylene and the 8-ring benzo[*a*]coronene (Figure 28), and the 9-ring naphtho[8,1,2-*abc*]coronene (Figure 29)—all from combining toluene, bi-toluyls, xylenes, benzene, and/or their radicals. Mechanisms of the types in Figures 24 and 26-29—in which the building blocks are particular aromatic units and not small species such as $C_2$—are more likely to lead to product distributions of the kind in Figure 4, in which a high degree of product selectivity is evident (*i.e.*, only certain species of a given ring number are produced and not others).

*Global Kinetics for PAH Formation and Parameters for the Pressure-Dependent Rate Constant*

The pressure-dependent product yield data of the type in Figures 10-23 permit us to determine the pressure dependency of the global kinetic rate constants for formation of PAH in supercritical toluene pyrolysis. For our global kinetic analysis, we assume that the rate of production of each product B is first order in the concentration of toluene A, so

$$d[B]/dt = k[A] \qquad (1)$$

where k is the global kinetic rate constant (in $sec^{-1}$) for the formation of B. For the range of conditions examined in our supercritical toluene pyrolysis experiments, the level of toluene conversion is very small, less than 1 %, so the concentration of A is effectively constant with time, at its initial value of $[A]_0$. Therefore, integration of (1) over time gives:

$$[B] = k[A]_0 t \qquad (2)$$

or

$$[B]/[A]_0 = kt \qquad (3)$$

where $[B]/[A]_0$ is just the yield of B, as plotted in Figures 10-23.

For constant temperature, the pressure dependency of the rate constant k is given [9] as:

$$k = A \exp[(-\Delta V^*/RT)p] \qquad (4)$$

where $A$ is the preexponential factor (in $sec^{-1}$) and $\Delta V^*$ is the activation volume (in L/mole), defined as the difference between the partial molar volume of the transition state and the partial molar volume of the reactants. Substitution of (4) into (3) gives:

$$[B]/[A]_0 = At\{\exp[(-\Delta V^*/RT)p]\} \qquad (5)$$

Therefore a set of product yield data at constant temperature and residence time but varying pressure lends itself to determining $\Delta V^*$ and $A$, if the data conform to the assumed first-order global kinetics.

Using the data from our supercritical toluene pyrolysis at 535 °C and 550 sec, we fit the experimentally measured yield/pressure data for each product to Equation (5), determining the values of $\Delta V^*$ and $A$ that best fit the data for each product species. A yield/pressure curve is then generated from the derived values of $\Delta V^*$ and $A$, to examine how well the experimental data conform to the assumed first-order behavior.

Figures 30-34 and Table 1 show the results of this exercise for the PAH product yield data from supercritical toluene pyrolysis at 535 °C and 550 sec. In Figures 30-34, each of the filled circles is an experimentally measured product yield. Each curve is the one generated from the values of $\Delta V^*$ and $A$ that best fit the data in the form of Equation (5). The close matching of the data points and curves for each of the PAH in Figures 30-34 shows that the data conform very well to the assumed first-order global kinetics model. The high values of the correlation coefficient $R^2$ in Table 1 show that all of the product PAH—from 1-ring to 9-ring aromatics—conform well to this type of first-order global kinetic treatment.

Table 1 also reports the values of ln $A$ and $\Delta V^*$ that best fit the experimental data for each product. The negative values of $\Delta V^*$ of course indicate that higher pressures favor formation of the PAH products, as the experiments demonstrate. The magnitudes of the $\Delta V^*$ values in Table 1 are typical for reactions in supercritical fluids (two orders of magnitude higher than for liquid-phase reactions) [6,9]. For an activation volume of -3L/mole at 535 °C, it takes only a 15.3-atm rise in pressure to double the formation rate of the product PAH; for an activation volume of -4 L/mole, the formation rate doubles with a pressure increase of only 11.5 atm. The activation

volumes in Table 1 are a good indicator of just how highly pressure-sensitive PAH formation is in the supercritical toluene pyrolysis environment. With respect to solid deposit formation, it may be significant to note from Table 1 that the largest PAH are the ones whose formation rates are the most sensitive to pressure.

*Pyrolysis of n-Heptane and Methylcyclohexane*

The supercritical pyrolysis reactor of Figure 1 has also been employed in experiments with *n*-heptane, a model fuel representative of aliphatic components of jet fuels, and methylcyclohexane, a model endothermic fuel. Under the conditions investigated—temperatures up to 570 °C, pressures up to 100 atm, and residence times up to 30 sec—pyrolysis of *n*-heptane has not produced detectable quantities of PAH or solid deposits. Longer residence times should be examined, though, before any conclusions are drawn about *n*-heptane—especially since the closely related alkane *n*-octane has proven to be prone to producing solid deposits in UTRC's scramjet test rigs [4].

For the case of methylcyclohexane, subjected to the same ranges of experimental conditions, analysis of the reaction products reveals that for the 30-sec residence time employed and the entire range of pressures investigated, PAH are not produced at detectable levels at temperatures $\leq$ 430 °C. At the highest temperatures of 530 and 570 °C, PAH are produced at all pressures. At the intermediate temperature of 470 °C, PAH are detected at all pressures but in only minimally detectable amounts at the lowest pressure of 20 atm.

As in the case of the supercritical toluene experiments, the supercritical pyrolysis experiments with methylcyclohexane show that an increase in pyrolysis temperature brings about an increase in PAH production as well as an increase in the molecular sizes of the PAH formed. Figure 35 depicts an HPLC chromatogram of the products from methylcyclohexane pyrolysis at 570 °C and 100 atm, the highest temperature and pressure examined. Even though Figure 35 contains some unresolved components (due to the high degree of alkylation), twenty-three PAH have been unequivocally identified among these methylcyclohexane pyrolysis products—all but two (2,3-dimethylnaphthalene and benzo[*a*]fluorene) of which are also observed as supercritical toluene

pyrolysis products in Figure 4. The UV spectral matches confirming the identities of two of the methylcyclohexane products of Figure 35, benzo[*a*]pyrene and anthanthrene, are displayed in Figure 36.

As illustrated in Figure 35, supercritical pyrolysis of methylcyclohexane at 570 °C and 100 atm produces a variety of PAH, ranging in size from one to seven aromatic rings, and including several classes of compounds: 10 benzenoid PAH (those with only six-membered rings), 3 fluoranthene benzologues (those with an internal five-membered ring), 3 indene benzologues (those with a five-membered ring containing a methylene carbon), and 6 methylated PAH. The high abundance of methylated PAH distinguishes these methylcyclohexane products from products of purely aromatic fuels [20] and undoubtedly results from the abundance of methyl fragments readily produced from pyrolysis of a hydrogen-rich endothermic fuel such as methylcyclohexane. Additional methylated PAH are thought to be among the products not yet identified in Figure 35 due to the coelution of species and the consequent superposition of peaks in the product components' UV spectra.

Similar again to the results of the toluene experiments, the supercritical pyrolysis experiments with methylcyclohexane show that pressure is a huge factor in determining PAH yields. Figures 37 and 38 illustrate the effect of pressure on the yields of 2-, 3-, and 4-ring PAH produced from methylcyclohexane pyrolysis at 530 °C and 30 sec. As these figures indicate, all PAH increase in yield as pressure is increased—the greatest jump occurring in the interval from 80 to 100 atm, just as in the case of toluene.

For methylcyclohexane, the increase of PAH production with increasing pressure can be tied to the findings of Stewart [10]. As proposed by Stewart [10] and demonstrated in Figure 39, methylcyclohexane pyrolysis produces an intermediate, the methylhexenyl radical, which either in the gas phase at atmospheric pressure or in the supercritical phase produces β-scission products such as ethene and propene. In the very dense environments characteristic of supercritical pressures, however, diffusion of β-scission products (away from one another) is impaired and collision processes are favored, enhancing carbon-carbon bond formation and facilitating the

production of cyclic structures. Under supercritical conditions, therefore, the intermediate methylhexenyl radical produces dimethylcyclopentane [10], a hydrocarbon containing a methylated five-membered ring. Such five-membered-ring species have been shown [10, 40] to undergo facile conversion to structures containing six-membered aromatic rings. It thus makes sense that the higher pressures that enhance production of five-membered-ring species also enhance production of PAH, as demonstrated in the methylcyclohexane experiments (Figures 37 and 38).

*Products of Supercritical Pyrolysis of JP-7*

The above results from our laboratory-scale supercritical pyrolysis reactor were discussed, in part, with Dr. Tim Edwards and his colleagues at Wright-Patterson Air Force Research Laboratory, during the Principal Investigator's visit there in February, 2002. Subsequent exchanges with Dr. Edwards and his sharing of scramjet test results on solid deposition prompted us to perform HPLC analyses on samples from the scramjet tests.

Figure 40 shows the results of our HPLC/UV analysis of products from JP-7 fuel subjected to supercritical conditions in a scramjet test rig [41] at UTRC in East Hartford, Connecticut. Due to the huge number of constituents in JP-7 fuel, the product mixture is of course extremely complex, as evidenced by the "hump" of not fully resolved components in the chromatogram of Figure 40. Despite this complexity, we are able to unequivocally identify, in this product sample, the 22 PAH whose structures appear in Figure 40. Except for 1-methylanthracene (whose signal would be obscured by bi-toluyls in Figure 4), all of the PAH in the supercritical JP-7 products of Figure 40 are also products of our supercritical toluene pyrolysis experiments; most are also in the methylcyclohexane PAH products of Figure 35. Relevance is thus established between our laboratory-scale supercritical pyrolysis experiments with the model fuels and the larger-scale scramjet tests with actual jet fuels. Dr. He Huang, Fuels Lab Leader at UTRC, who supplied the JP-7 product sample to us, is planning to visit our laboratory so that we might discuss our results and explore opportunities for collaboration.

## Summary of Results

*PAH from toluene pyrolysis.* Using a reactor specially designed for supercritical fuels pyrolysis studies, we have conducted supercritical pyrolysis experiments with the model fuel toluene at temperatures up to 585 °C, pressures up to 100 atm, and residence times up to 550 sec. Analyses of the reaction products by GC/FID/MS and by HPLC/UV, an isomer-specific technique ideally suited for the analysis of PAH (precursors to solid deposits), show that the major aromatic products of supercritical toluene pyrolysis are benzene, the xylenes, and the bi-toluyls—all of which can form without the breaking of toluene's aromatic ring. HPLC/UV analysis has unequivocally identified 27 individual PAH of up to 10 rings; for many of the 27, it is the first time that they have ever been identified as toluene products or as the products of supercritical pyrolysis of any fuel.

*Temperature sensitivity and solids formation.* The supercritical toluene pyrolysis experiments show that PAH production is extremely sensitive to temperature, especially at high pressures. Results at 100 atm and 550 sec show that at 480 °C, only bi-toluyls and 1- and 2-ring aromatics are formed; at 535 °C, yields of the bi-toluyls increase by a factor of 20, and PAH up to 10 rings are formed; at 585 °C, solid deposits form, plugging the reactor. Evidence is thus established that PAH are indeed precursors to the solid deposits.

*PAH product distribution.* The nature of the PAH product distribution from the supercritical conditions is hugely different from those of atmospheric-pressure gas-phase environments. Relative proportions of PAH within a given isomer family ( *e.g.*, $C_{14}H_{10}$, $C_{16}H_{10}$, and $C_{22}H_{12}$) are markedly different. The high pressures of the supercritical environment permit the formation, at relatively low pyrolysis temperatures, of large-ring-number PAH, which at atmospheric pressure would form only at temperatures many hundreds of degrees higher.

*PAH formation mechanisms.* The PAH product distribution from supercritical pyrolysis of toluene shows no evidence of the aromatic ring in the toluene structure ever having broken and no evidence of the $C_2$-addition mechanism commonly invoked for PAH growth in subcritical pyrolysis and combustion environments (*i.e.*, $C_2$-addition products such as cyclopenta-fused PAH

and ethynyl-PAH are not present). Condensation reactions, involving the addition of aromatic structures (*e.g.*, toluene, benzene, xylenes, toluene dimers, and their radicals) present in the reaction environment, followed by dehydrogenation, appear to be responsible for PAH formation in the supercritical toluene pyrolysis environment.

*Pressure sensitivity and global kinetics.* PAH yields are extremely sensitive to pressure, increasing exponentially as pressure exceeds the critical pressure. For each of the PAH at 535 °C, the experimentally measured yield/pressure data conform well to a first-order global kinetics model—permitting determination, for each product PAH, of the preexponential factor $A$ and the activation volume $\Delta V^*$ used in the pressure-dependent expression for the kinetic rate constant in supercritical reactions: $k = A \exp[(-\Delta V^*/RT)p]$. For most of the PAH, derived values of $\Delta V^*$ lie between -3 L/mole and -4 L/mole, signifying the doubling of PAH formation rates by pressure increases of only 15.3 or 11.5 atm, respectively. With respect to solid deposit formation, it is significant to note that the largest PAH are the ones whose formation rates are the most sensitive to pressure.

*Pyrolysis of other model fuels.* Under the ranges of experimental conditions examined, *n*-heptane does not produce measurable amounts of PAH or solid deposits, but longer residence times should still be examined. For methylcyclohexane, PAH are not produced at detectable levels at temperatures $\leq$ 430 °C; at temperatures $\geq$ 470 °C, PAH are produced at all pressures. The twenty-two individual PAH identified in the methylcyclohexane reaction products are also found in the toluene pyrolysis products. PAH yields from methylcyclohexane pyrolysis also exhibit the extreme sensitivities to temperature and pressure demonstrated by those from the toluene experiments.

*Relevance to jet fuels.* HPLC/UV analyses of the supercritical pyrolysis products of JP-7, supplied by Dr. He Huang of UTRC, show that most or all of the PAH identified as products from JP-7 are also among the PAH produced in our supercritical toluene pyrolysis experiments. Relevance is thus established between our laboratory-scale supercritical pyrolysis experiments with the model fuels and the larger-scale scramjet tests with actual jet fuels.

## Future Work

The above findings from our supercritical fuels pyrolysis research suggest the need for additional experiments along the following lines:

(1) Assuming global first-order kinetics for PAH formation, we have determined values of the kinetic parameters $A$ and $\Delta V^*$ for toluene pyrolysis at 535 °C and 550 sec. Toluene pyrolysis experiments at additional temperatures need to be conducted in order to determine how $A$ and $\Delta V^*$ vary with temperature.

(2) The toluene results to date show that at 550 sec, 100 atm, and 535 °C, toluene conversion is low and yields of large PAH are on the order of only 10 μg/g. At a temperature just 50 °C higher, though, solid deposits are produced in sufficient amount to plug the reactor. In order to better understand how the transition occurs from small amounts of large PAH to large amounts of solid deposits, additional toluene pyrolysis experiments need to be performed at small increments of pressure (~5 atm) and at small increments of temperature (~10 °C) within the high-temperature (535-585 °C), high-pressure (60-100 atm) ranges of this "near incipient" zone for solids formation.

(3) Results have been obtained on PAH and solid deposit formation from toluene, an aromatic component of jet fuels. Jet fuels contain aliphatic as well as aromatic components, however. In order to examine how PAH formation from an aromatic component of jet fuel may be affected by the presence of aliphatic components, pyrolysis experiments should be conducted with toluene doped with varying amounts of *n*-heptane.

(4) One of the important findings of the supercritical toluene experiments is that PAH formation in that environment does not require breaking of the aromatic ring in toluene. Instead the aromatic ring remains in tact to serve as a building unit for the PAH, and presumably eventually the solid deposits. If the same result holds for other aromatic components of jet fuels, then larger-ring-number aromatic components, though present in smaller amounts, could play significant roles in the formation of large PAH and solids. In order to examine this question, pyrolysis experiments should be conducted with 1-methylnaphthalene, a 2-ring PAH identified in jet fuels [42], to see (a) if even larger PAH than ovalene (the largest one identified in the toluene products) are formed, (b) if less severe conditions (lower T, p, t) are needed to produce high-ring-number PAH; and (c) if solid deposits are formed more readily than in the case of toluene.

(5) Pyrolysis experiments with *n*-heptane and with methylcyclohexane need to be conducted at longer residence times in order to explore conditions more likely to foster solid deposit formation.

## Presentation and Publication of Research Results

Our results from the supercritical pyrolysis research are the subjects of two papers that are currently in preparation for submission to journals. In addition to the AFOSR Contractors' Review meetings, the results have been or will be presented at the following conferences:

Ledesma, E. B., Sivo, J. A., and Wornat, M. J., "Polycyclic Aromatic Hydrocarbons Produced from the Supercritical Pyrolysis of Methylcyclohexane," Two-Hundred Twenty-First National Meeting of the American Chemical Society, San Diego, California, April, 2001.

Ledesma, E. B., Felton, P. G., Sivo, J. A., and Wornat, M. J., "Pyrolysis of Toluene under Supercritical Conditions," Twenty-Ninth International Symposium on Combustion, Sapporo, Japan, July, 2002.

Wornat, M. J., Ledesma, E. B., Felton, P. G., and Sivo, J. A., "Polycyclic Aromatic Hydrocarbons from the Supercritical Pyrolysis of Toluene," Two-Hundred Twenty-Fifth National Meeting of the American Chemical Society, New Orleans, Louisiana, March, 2003.

Wornat, M. J., Ledesma, E. B., Felton, P. G., and Sivo, J. A., "Pressure-Dependent Global Kinetics Rate Parameters for the Formation of PAH from Supercritical Toluene Pyrolysis," Eighth International Congress on Combustion By-Products," Umea, Sweden, June, 2003.

Ledesma, E. B., Felton, P. G., Sivo, J. A., and Wornat, M. J., "Formation of Polycyclic Aromatic Hydrocarbons from the Supercritical Pyrolysis of Toluene," Nineteenth International Symposium on Polycyclic Aromatic Compounds," Amsterdam, the Netherlands, September, 2003.

## Acknowledgements

We gratefully acknowledge the AFOSR, Grant Number F49620-00-1-0298, for support of this research. We thank Dr. Elmer Ledesma, Dr. Philip Felton, Mr. Nathan Marsh, and Mr. Joseph Sivo for technical contributions to this work. We also thank the following for reference standards and/or UV spectra of PAH: Dr. Arthur Lafleur and Ms. Elaine Plummer, of the Massachusetts Institute of Technology; Professor Maximilian Zander, of Rütgerswerke; and Dr. John Fetzer, of Chevron Research.

## References

1. Harrison, W. E. III, *Aircraft Thermal Management*: Report of the Joint WRDC/ASD Aircraft Thermal Management Working Group, 1990. WRDC-TR-90-2021.

2. Heneghan, S. P., Zabarnick, S, Ballal, D. R., and Harrison, W. E. III, *Journal of Energy Resources Technology* **1996**, *118*, 170-179.

3. Edwards, T., and Zabarnick, *Industrial and Engineering Chemistry Research* **1993** *32*, 3117-3122.

4. Edwards, T., personal communication, AFRL, Wright-Patterson, Ohio, June 12, 2002.

5. Melius, C. F., Bergan, N. E., and Shepherd, J. E., *Proceedings of the Combustion Institute* **1990**, *23,* 217-223.

6. Johnston, K. P., and Haynes, C., *AIChE Journal* **1987**, *33*, 2017-2026.

7. Paulaitis, M. E., and Alexander, G. C., *Pure and Applied Chemistry* **1987**, *59*, 61-68.

8. Helling, R. H., and Tester, J. W., *Energy & Fuels* **1987**, *1*, 417-423.

9. Eckert, C. A., Knutson, B. E., and Debenedetti, P. G., *Nature* **1996**, *383*, 313-318.

10. Stewart, J. F., "Supercritical Pyrolysis of Endothermic Fuels," Ph.D. Thesis, Department of Mechanical and Aerospace Engineering, Princeton University, **1999**.

11. Wornat, M. J., Glassman, I., Stewart, J. F., Zeppieri, S. P., Ledesma, E. B., Sivo, J. A., and Marsh, N. D., "Fuels Combustion Research: Supercritical Fuel Pyrolysis," abstract from Army Research Office and Air Force Office of Scientific Research 2000 Contractors' Meeting in Chemical Propulsion, Santa Fe, New Mexico, June, 2000.

12. Stewart, J. F., Brezinsky, K., and Glassman, I., *Combustion Science and Technology* **1998**, *136*, 373.

13. Davis, G. D., "An Experimental Study of Supercritical Methylcyclohexane Pyrolysis," M.S.E. Thesis, Department of Mechanical and Aerospace Engineering, Princeton University, **1994**.

14. Wornat, M. J., Ledesma, E. B., Sivo, J. A., and Marsh, N. D., "Fuels Combustion Research: Supercritical Fuel Pyrolysis," abstract from Army Research Office and Air Force Office of Scientific Research 2001 Contractors' Meeting in Chemical Propulsion, Los Angeles, California, June, 2001, pp. 149-152.

15. Wornat, M. J., Ledesma, E. B., Felton, P. G., Sivo, J. A., and Marsh, N. D., "Fuels Combustion Research: Supercritical Fuel Pyrolysis," abstract from Army Research Office and Air Force Office of Scientific Research 2002 Contractors' Meeting in Chemical Propulsion, Dayton, Ohio, June, 2002, pp. 69-72.

16. Darrah, S., "Jet Fuel Deoxygenation," AFWAL-TR-88-2081 (1988).

17. Edwards, T., Gord, J., and Bunker, C., "Advanced Supercritical Fuels," abstract from Army Research Office and Air Force Office of Scientific Research 2001 Contractors' Meeting in Chemical Propulsion, Los Angeles, California, June, 2001, pp. 78-81.

18. Cutler, A. H., Antal, M. J., and Jones, M., *Industrial and Engineering Chemistry Research* **1988** *27*, 691-697.

19. Lee, J. C. Y., Ph.D. Thesis, Department of Mechanical and Aerospace Engineering, Princeton University, **1996**.

20. Wornat, M. J.; Sarofim, A. F.; Lafleur, A. L. *Proceedings of the Combustion Institute* **1992**, *24*, 955-963.

21. Wornat, M. J.; Lafleur, A. L.; Sarofim, A. F. *Polycyclic Aromatic Compounds* **1993**, *3*, 149.

22. Schmidt, W; Grimmer, G.; Jacob, J; Dettbarn, G.; Naujack, K.-W. *Fresnius' Zeitschrift für Anal. Chem.* **1987**, *326*, 401.

23. Wornat, M. J.; Vernaglia, B. A.; Lafleur, A. L.; Plummer, E. F.; Taghizadeh, K.; Nelson, P. F.; Li, C.-Z.; Necula, A.; Scott, L. T. *Proceedings of the Combustion Institute* **1998**, *27*, 1677-1686.

24. Wornat, M. J.; Ledesma, E. B.; Sandrowitz, A. K.; Roth, M. J.; Dawsey, S. M.; Qiao, Y. L.; Chen, W. *Environmental Science & Technology* **2001**, *35*, 1943-1952.

25. Ledesma, E. B.; Kalish, M. A.; Nelson, P. F.; Wornat, M. J.; Mackie, J. C. *Fuel* **2000**, *79*, 1801-1814.

26. Vernaglia, B. A., Wornat, M. J., Li, C. -Z., and Nelson, P. F., *Proceedings of the Combustion Institute* **1996**, *26,* 3287-3294.

27. Wornat, M. J.; Vriesendorp, F. J. J.; Lafleur, A. L.; Plummer, E. F.; Necula, A.; Scott, L. T. *Polycyclic Aromatic Compounds* **1999**, *13*, 221-240.

28. Marsh, N. D.; Zhu, D.; Wornat, M. J. *Proceedings of the Combustion Institute* **1998**, *27*, 1897.

29. Wornat, M. J., Ledesma, E. B., Marsh, N. D., Sandrowitz, A. K., *Fuel* **2001**, *80*, 1711.

30. Colket, M. B., and Seery, D. J., *Proceedings of the Combustion Institute* **1994**, *25,* 883.

31. Badger, G. M. and Spotswood, T. M., *Journal of the Chemical Society* **1960**,*1960*,4420.

32. Fetzer, J. C., and Kershaw, J. R., *Fuel* **1995**,*74,* 1533-1536.

33. Lafleur, A. L., Taghizadeh, K., Howard, J. B., Anacleto, J. F., and Quilliam, M. A., *Journal of the American Society of Mass Spectrometry* **1996***7,* 276-286.

34. Bockhorn, H.; Fetting, F.; Wenz, H. W. *Berichte Der Bunsen-Gesellschaft-Physical Chemistry Chemical Physics* **1983**, *87*, 1067-1073.

35. Frenklach, M.; Clary, D. W.; Gardiner, W. C. J.; Stein, S. E. *Proceedings of the Combustion Institute* **1984**, *20*, 887-901.

36. Ledesma, E. B.; Kalish, M. A.; Wornat, M. J.; Nelson, P. F.; Mackie, J. C. *Energy & Fuels* **1999**, *13*, 1167-1172.

37. Marsh, N. D.; Wornat, M. J.; Scott, L. T.; Necula, A.; Lafleur, A. L.; Plummer, E. F. *Polycyclic Aromatic Compounds* **1999**, *13*, 379-402.

38. Wornat, M. J.; Ledesma, E. B. *Polycyclic Aromatic Compounds* **2000**, *18*, 129.

39. Marsh, N. D.; Wornat, M. J. *Proceedings of the Combustion Institute* **2000**, *28*, 2585-2592.

40. Glassman, I. *Combustion*, Third Edition. San Diego: Academic Press, **1997**.

41. Huang, H., Spadaccini, L. J., and Sobel, D. R., "Fuel-Cooled Thermal Managment for Advanced Aero Engines," *Proceedings of TURBO EXPO 2002*, ASME Turbo Expo: Land, Sea & Air. Amsterdam, the Netherlands, June, 2002.

42. Bernabei, M., Reda, R., Galiero, R., and Bocchinfuso, G., *Journal of Chromatography A* **2003**, *985*, 197-203.

**Table 1.** Kinetic parameters, the pre-exponential factor $A$ and the activation volume $\Delta V^*$, determined for individual PAH produced by toluene pyrolysis at 535 °C, 550 sec, and pressures from 20 to 100 atm. The parameters are used in the pressure-dependent expression for the kinetic rate constant, Equation (4) in the text: $k=A\exp[(-\Delta V^*/RT)p]$. $R^2$ is the correlation coefficient for how well the experimentally measured yield data match the assumed first-order global kinetics, Equation (5) in the text.

| Name | ln $A$ ($s^{-1}$) | $\Delta V^*$ (L $mol^{-1}$) | $R^2$ |
|---|---|---|---|
| **1- and 2-ring aromatics** | | | |
| benzene | -18.2 | -2.95 | 0.993 |
| indene | -21.8 | -2.93 | 0.963 |
| naphthalene | -20.0 | -2.54 | 0.980 |
| 1-methylnaphthalene | -23.6 | -3.49 | 0.972 |
| 2-methylnaphthalene | -22.1 | -3.83 | 0.990 |
| diphenylmethane | -19.3 | -2.20 | 0.983 |
| **3-ring PAH** | | | |
| flourene | -25.3 | -4.03 | 0.988 |
| phenanthrene | -23.1 | -3.15 | 0.993 |
| anthracene | -21.4 | -2.61 | 0.989 |
| **4-ring PAH** | | | |
| flouranthene | -26.1 | -3.75 | 0.997 |
| pyrene | -23.3 | -3.64 | 0.997 |
| benz[*a*]anthracene | -24.7 | -2.96 | 0.992 |
| chrysene | -25.3 | -2.88 | 0.982 |
| **5- and 6-ring PAH** | | | |
| benzo[*a*]pyrene | -25.6 | -3.66 | 0.998 |
| indeno[1,2,3-*cd*]pyrene | -25.5 | -3.06 | 0.989 |
| benzo[*ghi*]perylene | -24.5 | -3.74 | 0.998 |
| **7-, 8-, and 9-ring PAH** | | | |
| coronene | -23.6 | -3.41 | 0.994 |
| 1-methylcoronene | -23.8 | -3.05 | 0.969 |
| benzo[*a*]coronene | -30.2 | -5.64 | 0.999 |
| naphtho[8,1,2-*abc*]coronene | -30.2 | -6.56 | 0.999 |

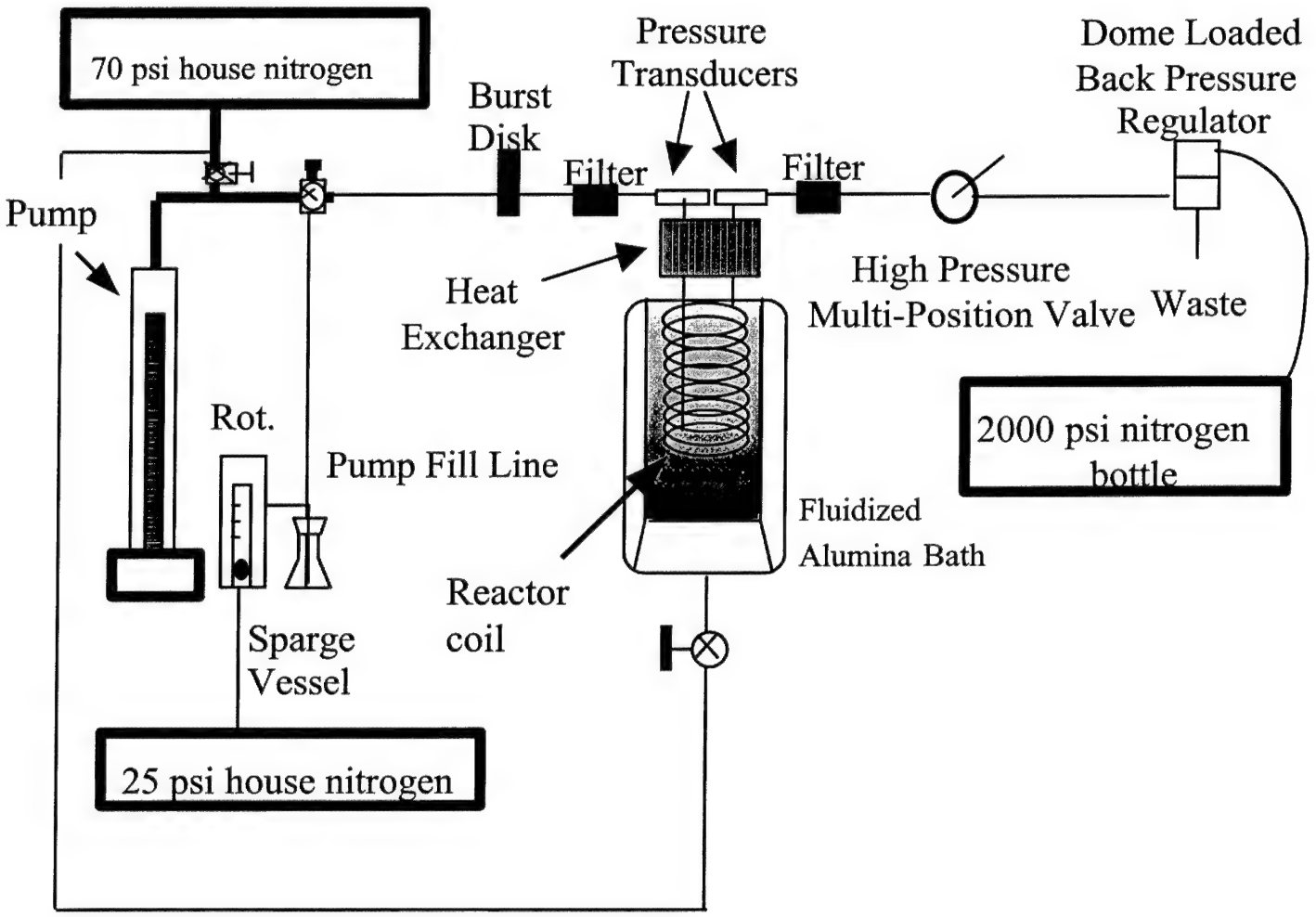


**Figure 1.** Supercritical pyrolysis reactor system. Adapted from Stewart [Stewart, 1999].

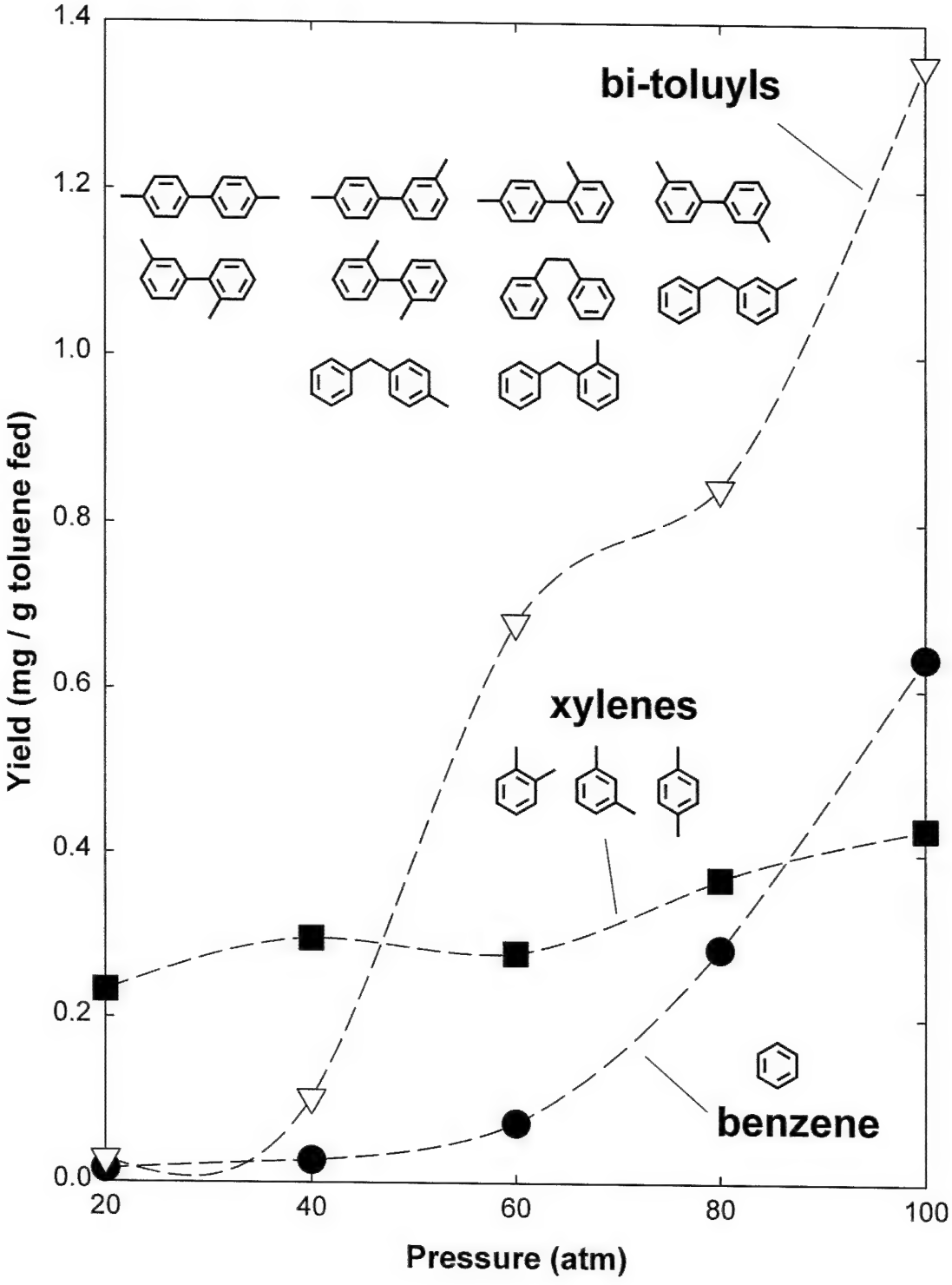


**Figure 2.** Pressure dependency of yields of major products of toluene pyrolysis at 535 $^{o}$C and 550 sec.

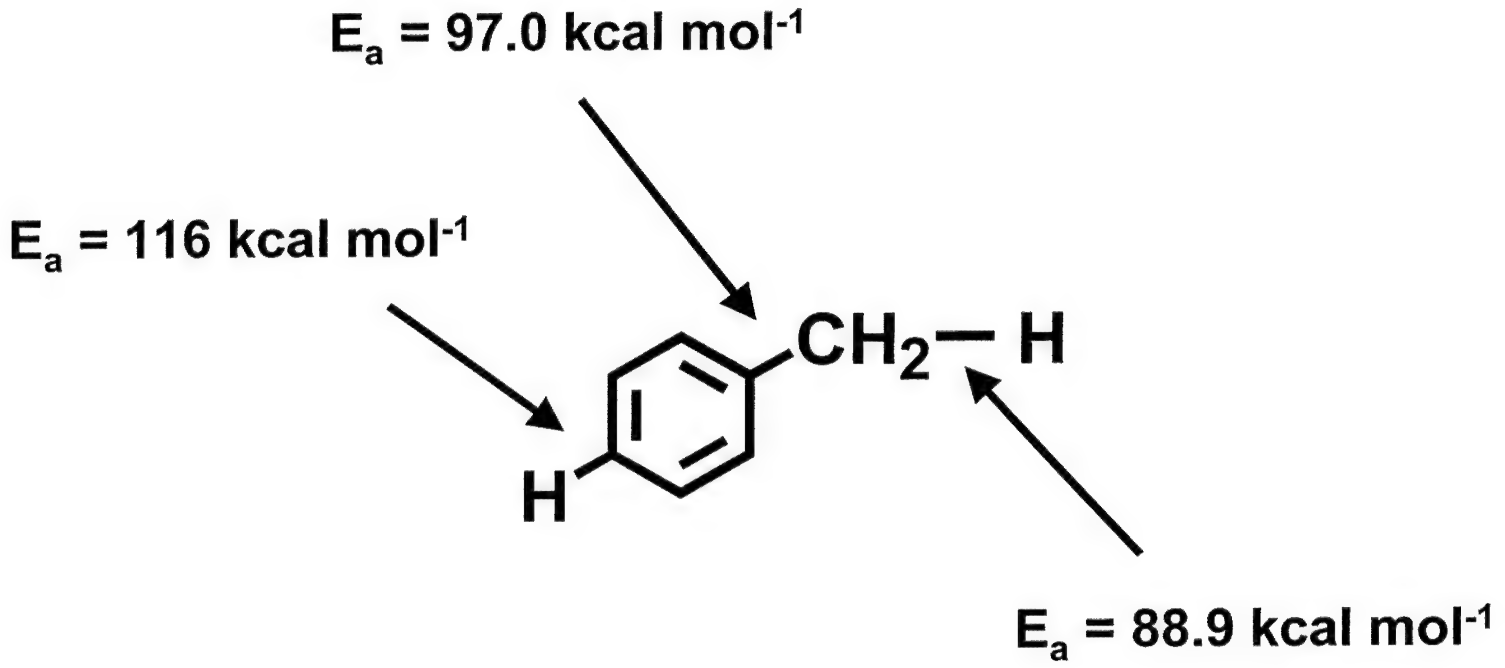


**Figure 3.** Activation energies for scission of indicated bonds in toluene [Colket and Seery, 1994].

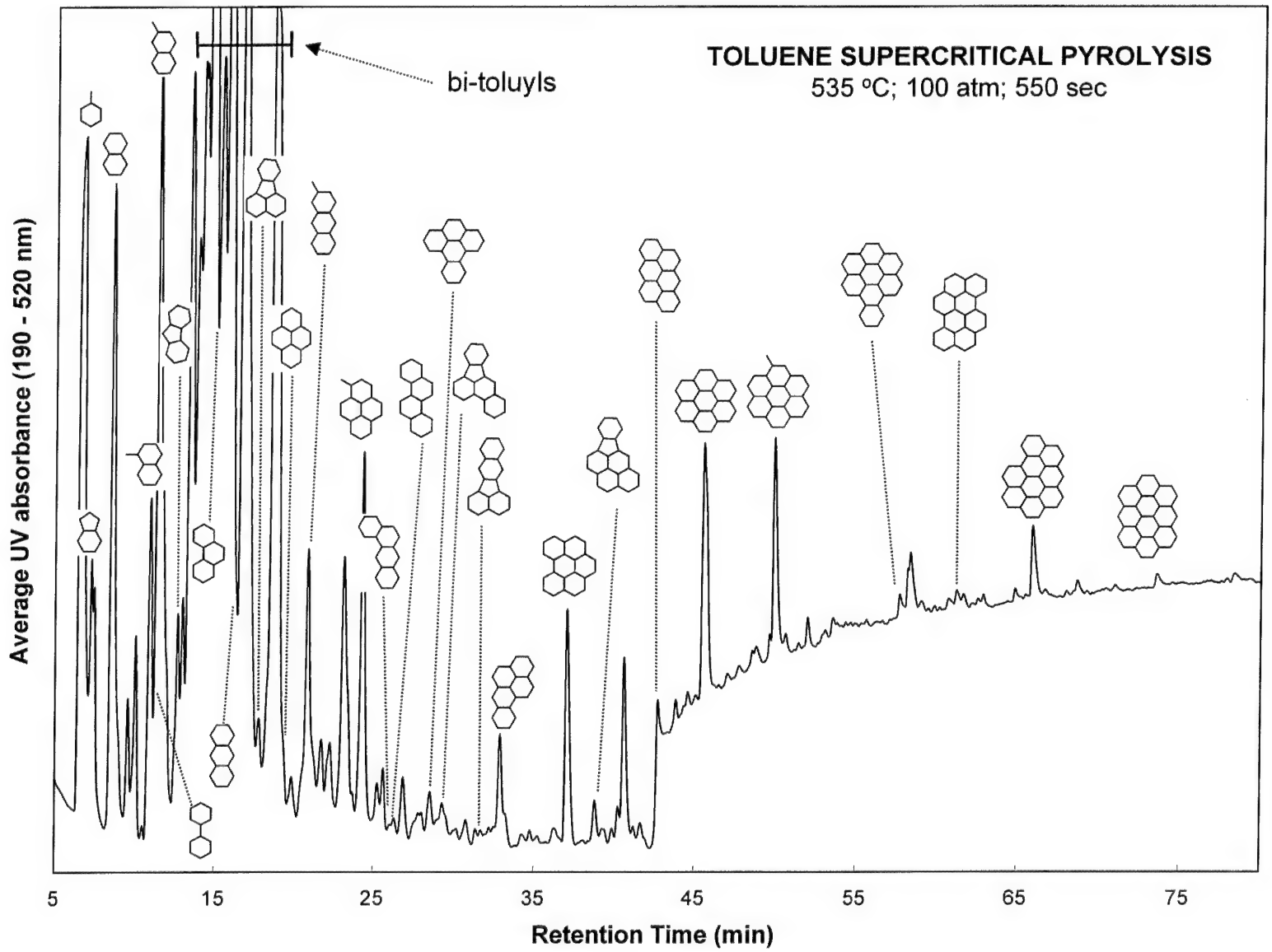


**Figure 4.** HPLC chromatogram of products of supercritical toluene pyrolysis at 535 °C and 100 atm. Rise in baseline at ~ 43 minutes is due to a change in the HPLC mobile phase to the UV-absorbing dichloromethane. Identified components, from left to right, are: toluene, indene, naphthalene, 1-methylnaphthalene, biphenyl, 2-methylnaphthalene, fluorene, phenanthrene, anthracene, fluoranthene, pyrene, 2-methylanthracene, 1-methylpyrene, benz[*a*]anthracene, chrysene, benzo[*e*]pyrene, benzo[*b*]fluoranthene, benzo[*k*]fluoranthene, benzo[*a*]pyrene, benzo[*ghi*]perylene, indeno[1,2,3-*cd*]pyrene, anthanthrene, coronene, 1-methylcoronene, benzo[*a*]coronene, benzo[*pqr*]naphtho[8,1,2-*bcd*]perylene, naphtho[8,1,2-*abc*]coronene, ovalene.

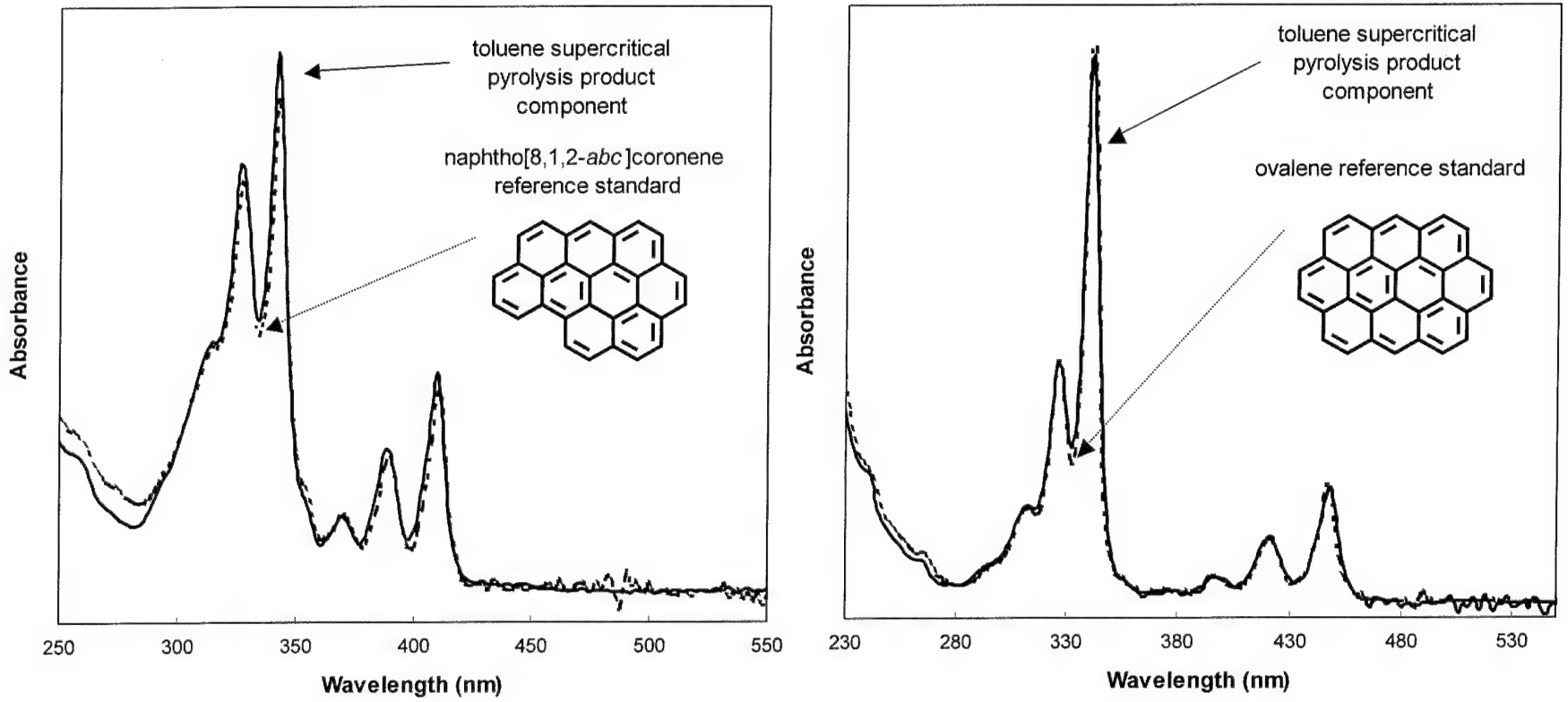


**Figure 5.** Matching UV absorption spectra of reference standards (dashed lines) and toluene pyrolysis product components (solid lines): naphtho[8,1,2-*abc*]coronene and ovalene. Synthesized reference standards provided by Dr. John Fetzer and Professor Maximillan Zander.

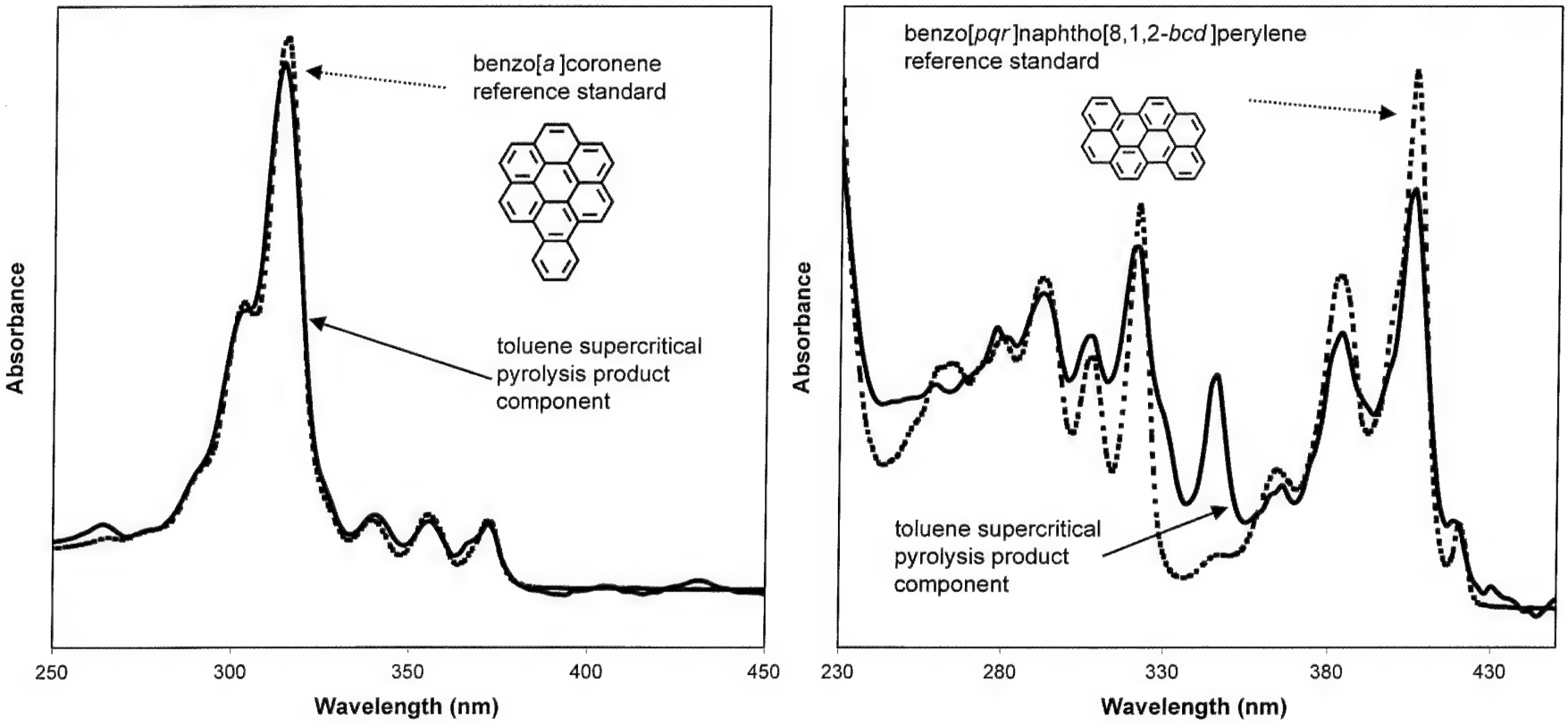


**Figure 6.** Matching UV absorption spectra of reference standards (dashed lines) and toluene pyrolysis product components (solid lines): benzo[*a*]coronene and benzo[*pqr*]naphtho[8,1,2-*bcd*]perylene. Synthesized reference standards provided by Dr. John Fetzer and Professor Maximillan Zander. The peak at ~ 350 nm in the product component spectrum on the right corresponds to interference from an unidentified co-eluting toluene product component.

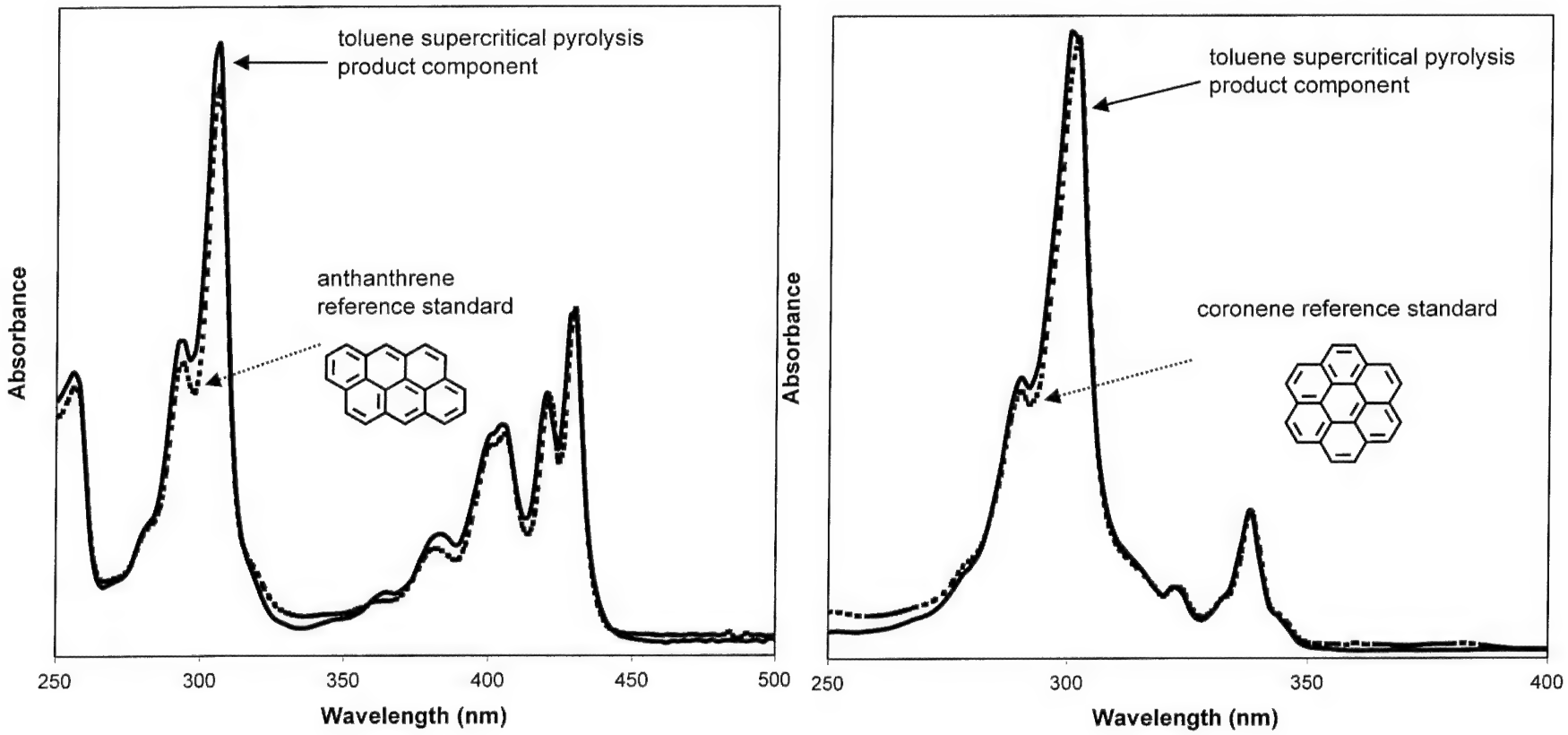


**Figure 7.** Matching UV absorption spectra of reference standards (dashed lines) and toluene pyrolysis product components (solid lines): anthanthrene and coronene.

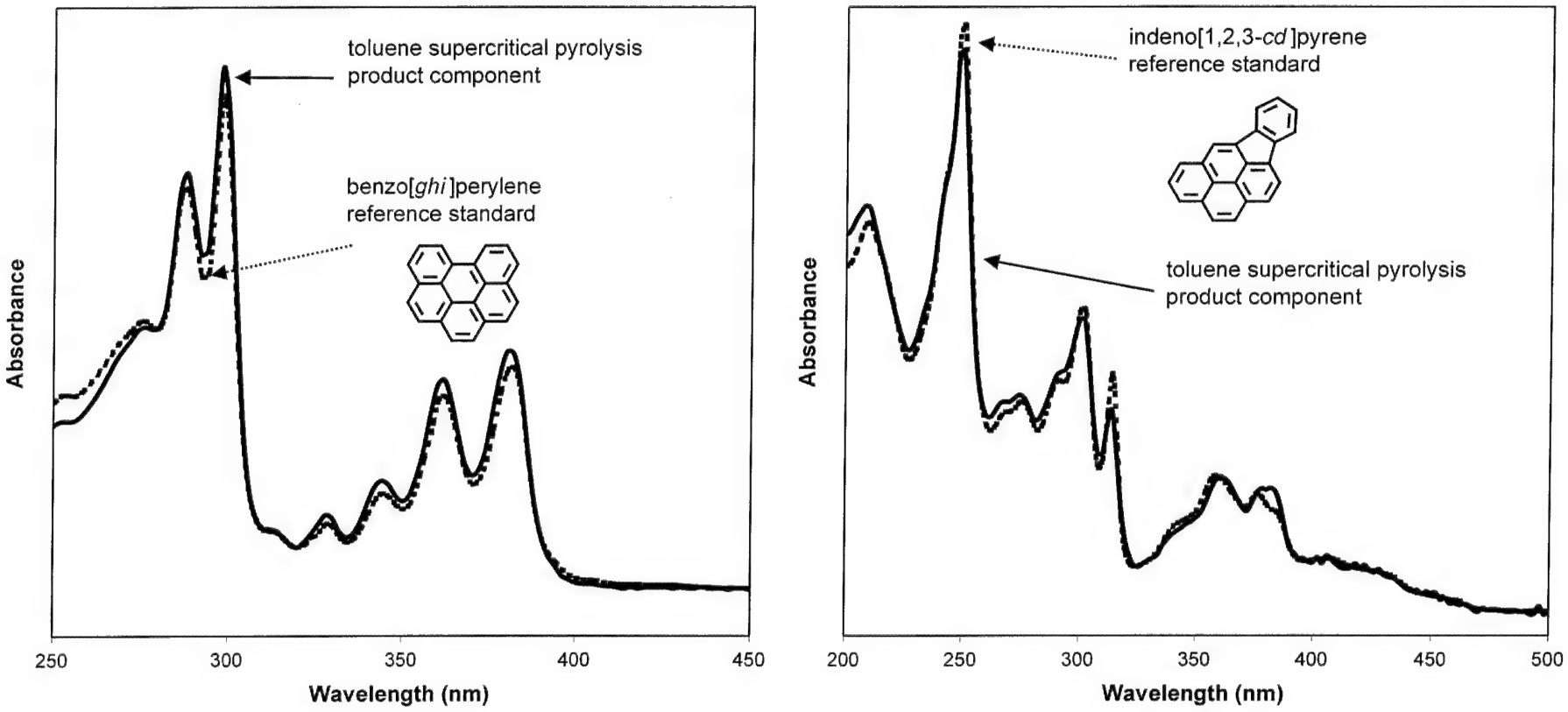


**Figure 8.** Matching UV absorption spectra of reference standards (dashed lines) and toluene pyrolysis product components (solid lines): benzo[*ghi*]perylene and indeno[1,2,3-*cd*]pyrene.

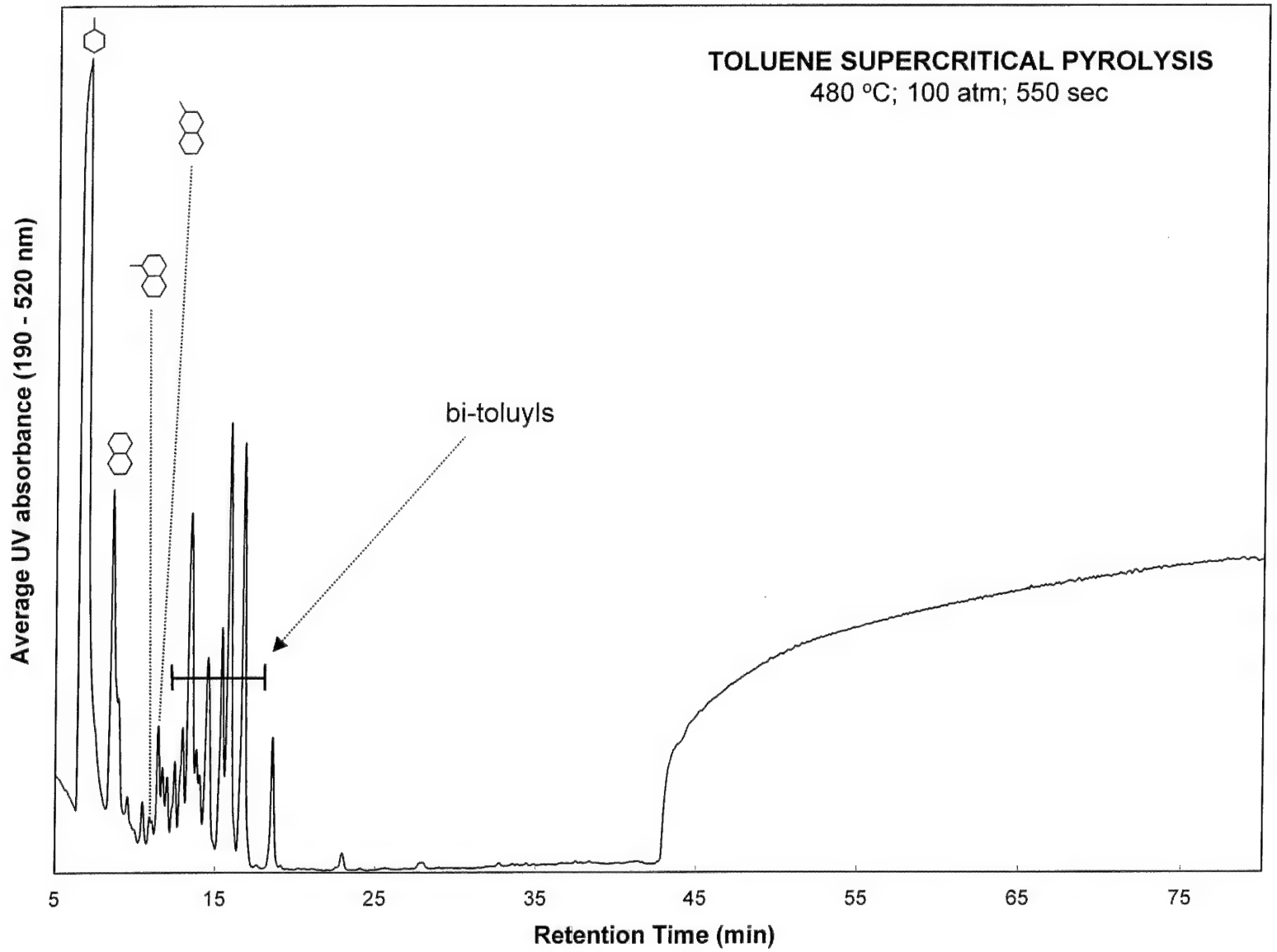


**Figure 9.** HPLC chromatogram of products of supercritical toluene pyrolysis at 480 °C and 100 atm. Rise in baseline at ~ 43 minutes is due to a change in the HPLC mobile phase to the UV-absorbing dichloromethane. Identified components, from left to right, are: toluene, naphthalene, 1-methylnaphthalene, 2-methylnaphthalene, bi-toluyls.

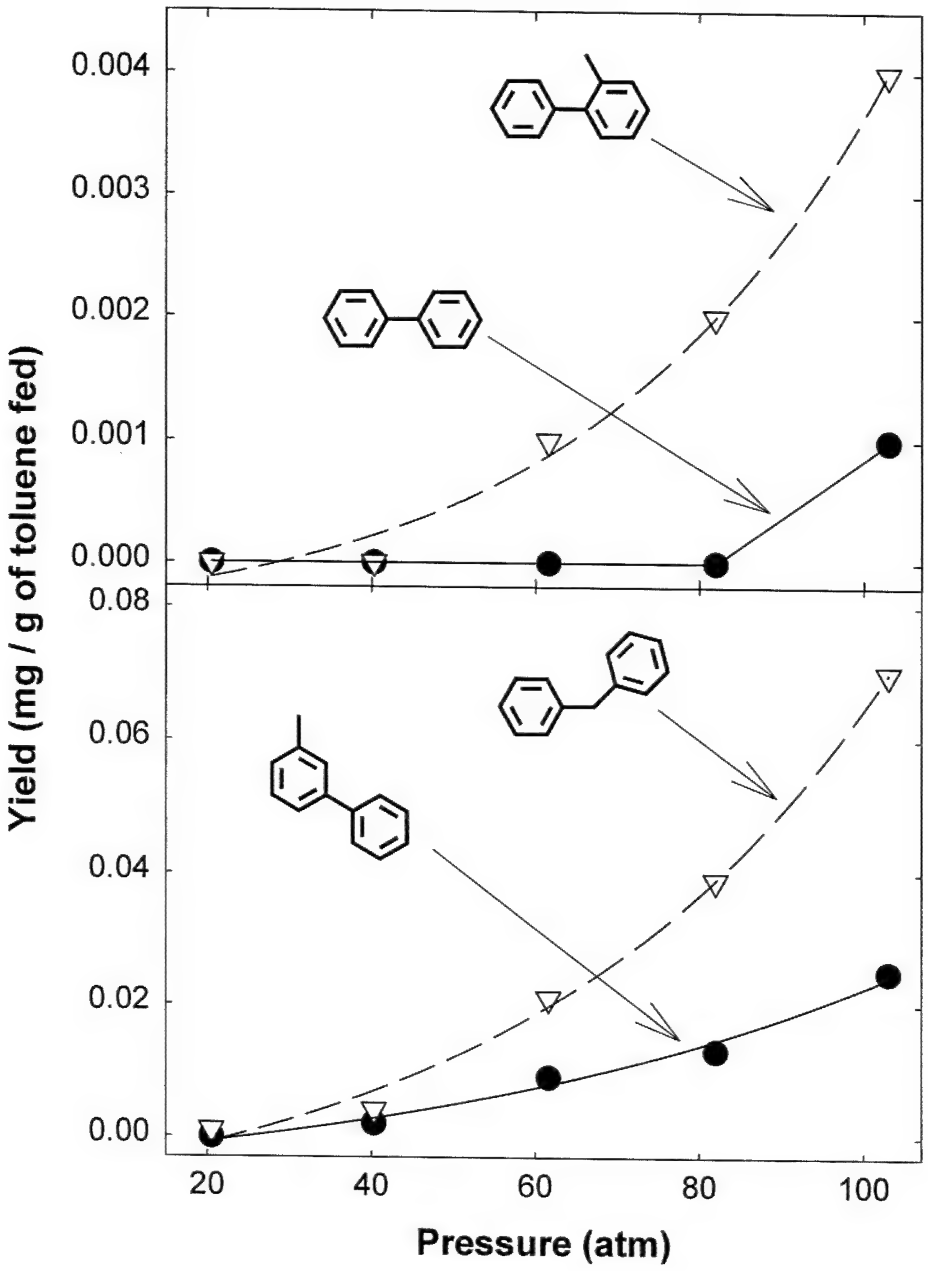


**Figure 10.** Yields of biphenyl and three phenyl-toluyls, as functions of pressure, from toluene pyrolysis at 535 °C and 550 sec.

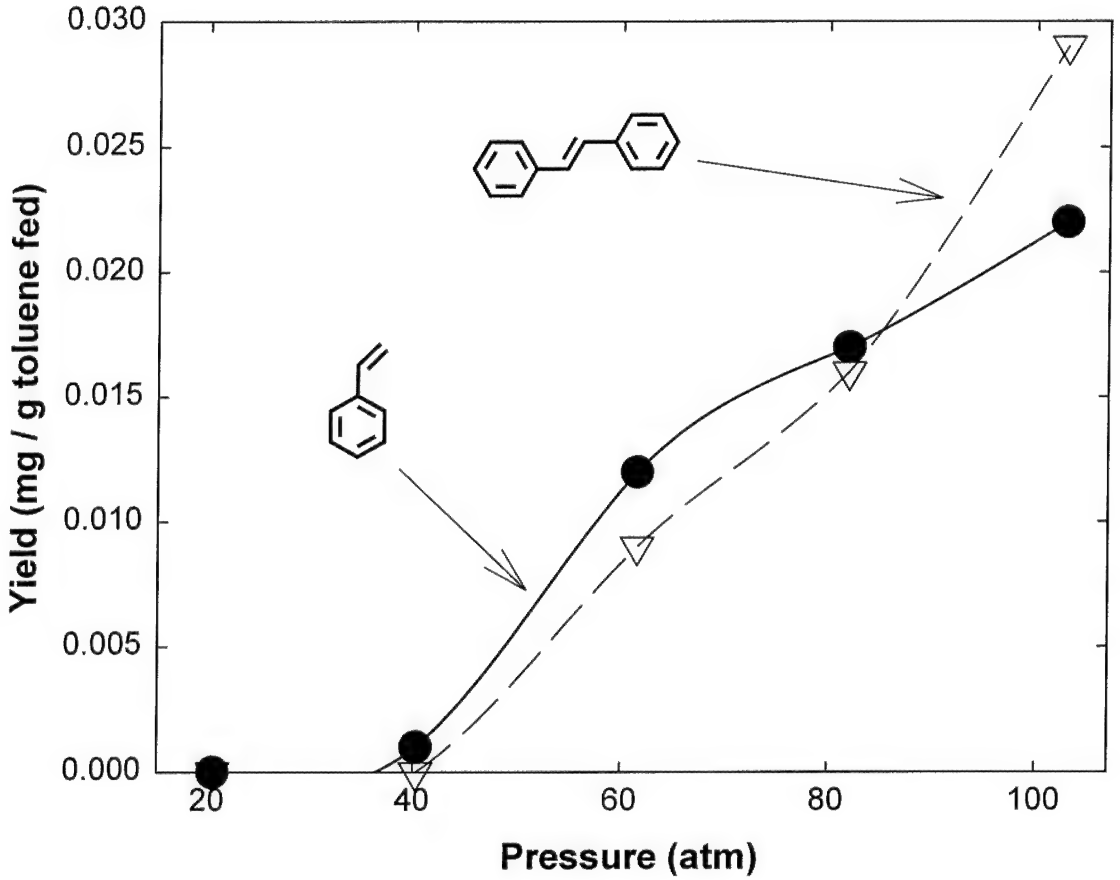


**Figure 11.** Yields of styrene and stilbene, as functions of pressure, from toluene pyrolysis at 535 °C and 550 sec.

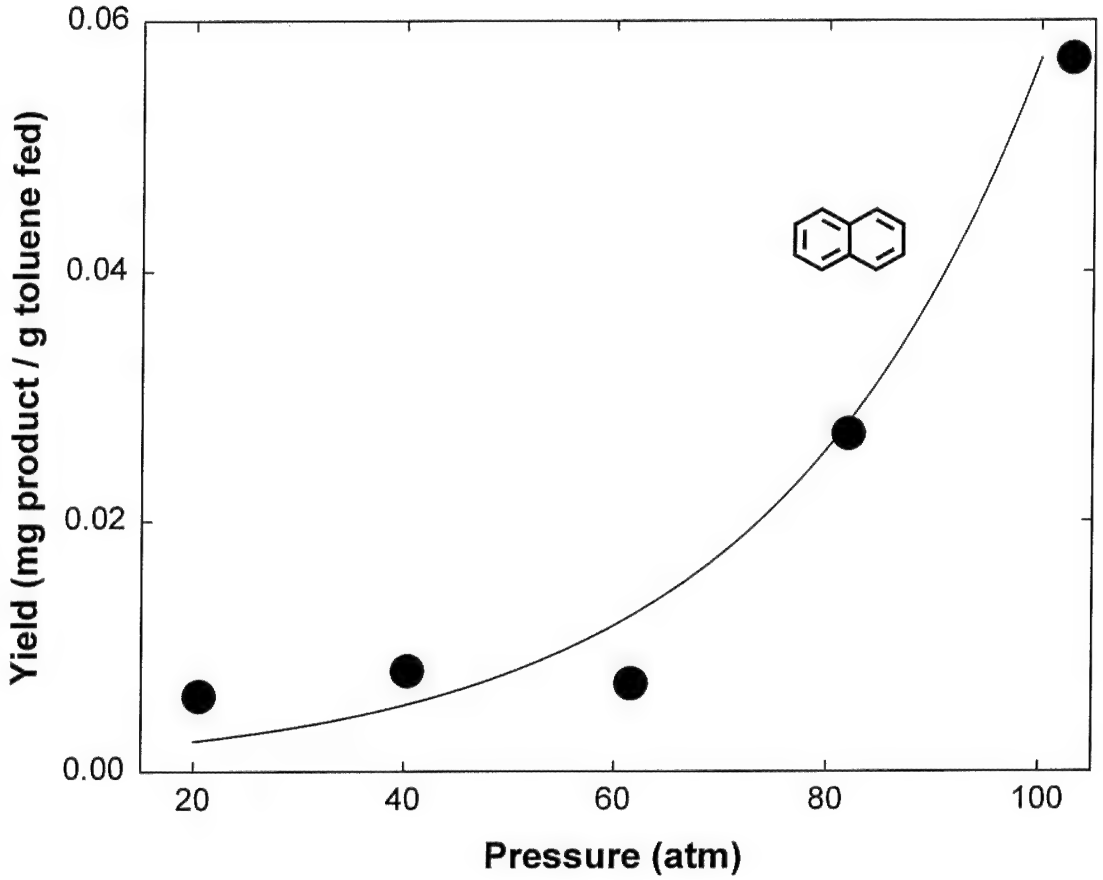


**Figure 12.** Yield of naphthalene, as a function of pressure, from toluene pyrolysis at 535 °C and 550 sec.

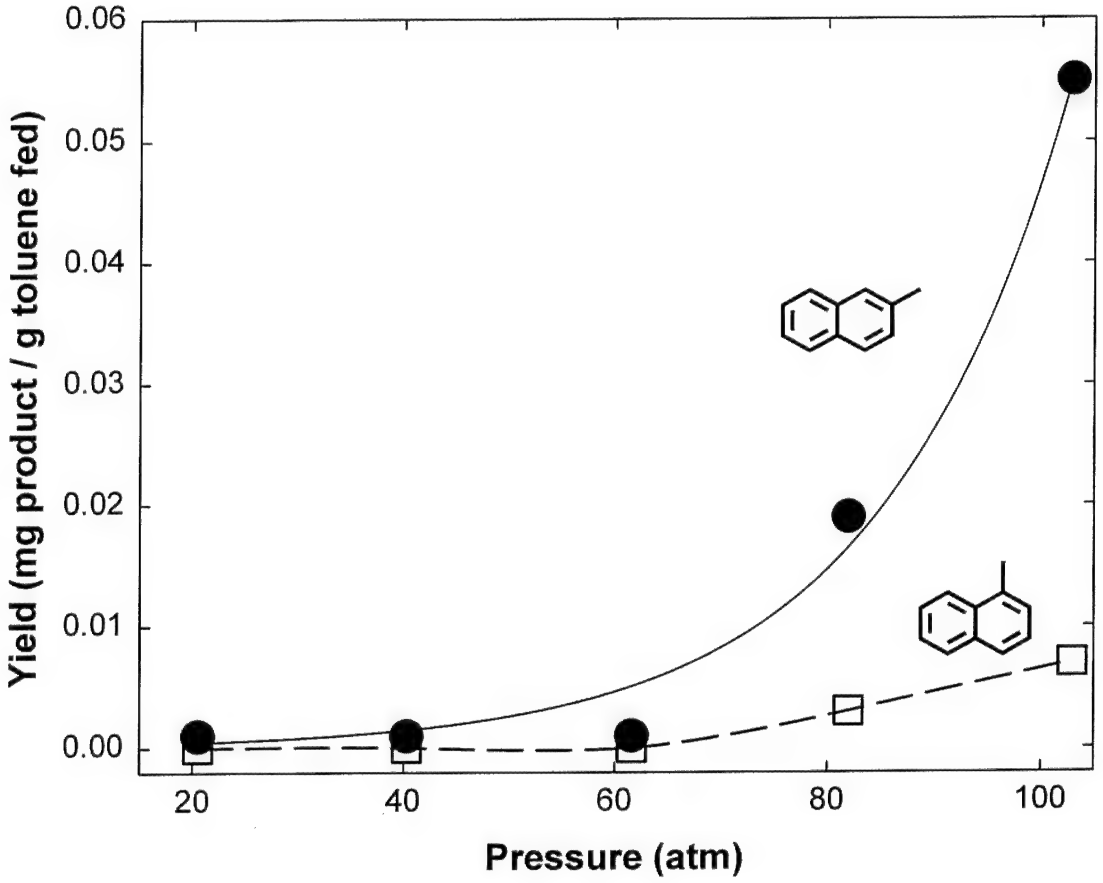


**Figure 13.** Yields of 1-methylnaphthalene and 2-methylnaphthalene, as functions of pressure, from toluene pyrolysis at 535 °C and 550 sec.

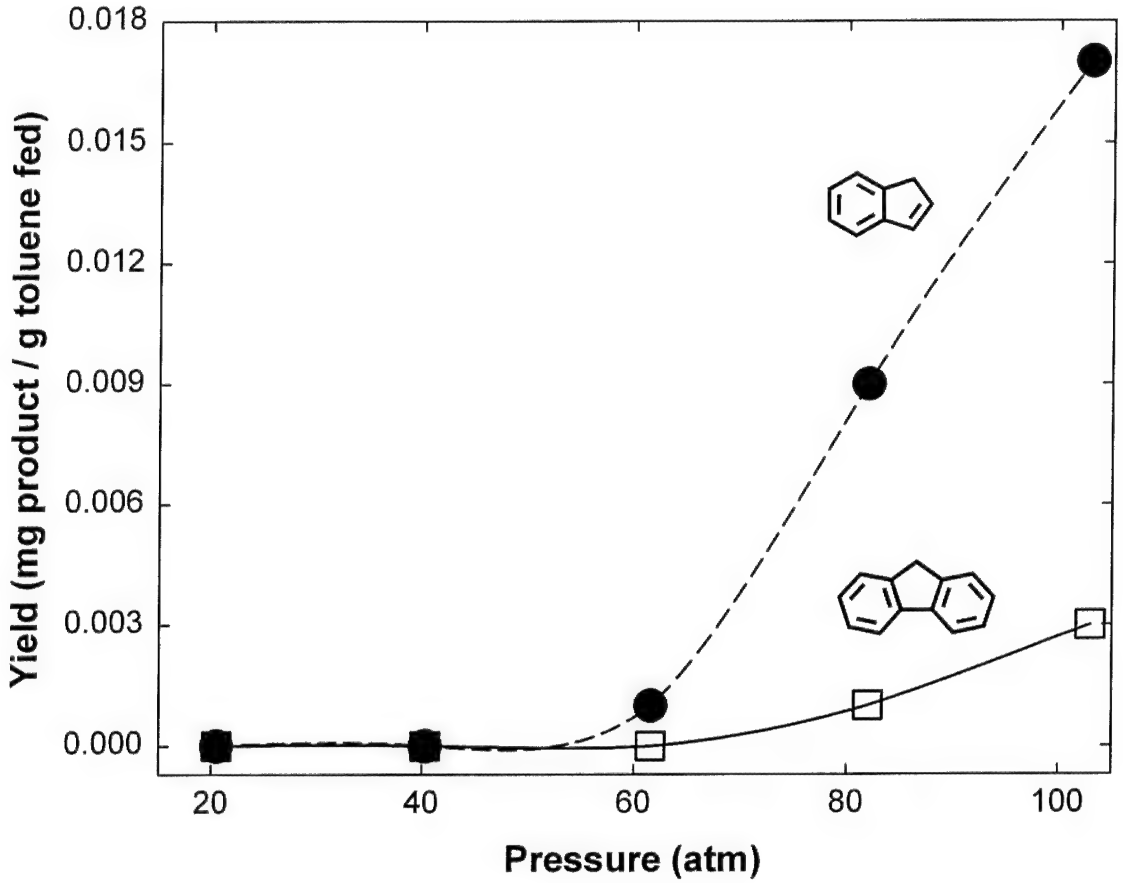


**Figure 14.** Yields of indene and fluorene, as functions of pressure, from toluene pyrolysis at 535 °C and 550 sec.

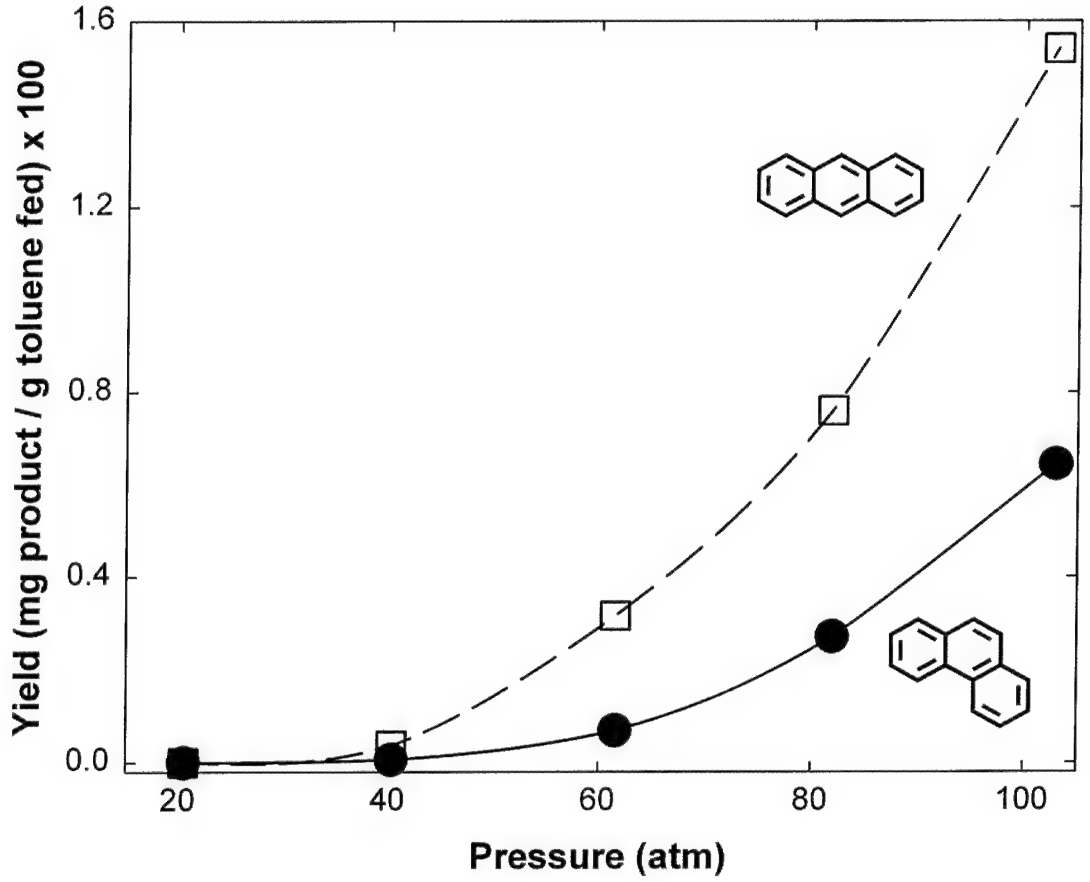


**Figure 15.** Yields of anthracene and phenanthrene, as functions of pressure, from toluene pyrolysis at 535 °C and 550 sec.

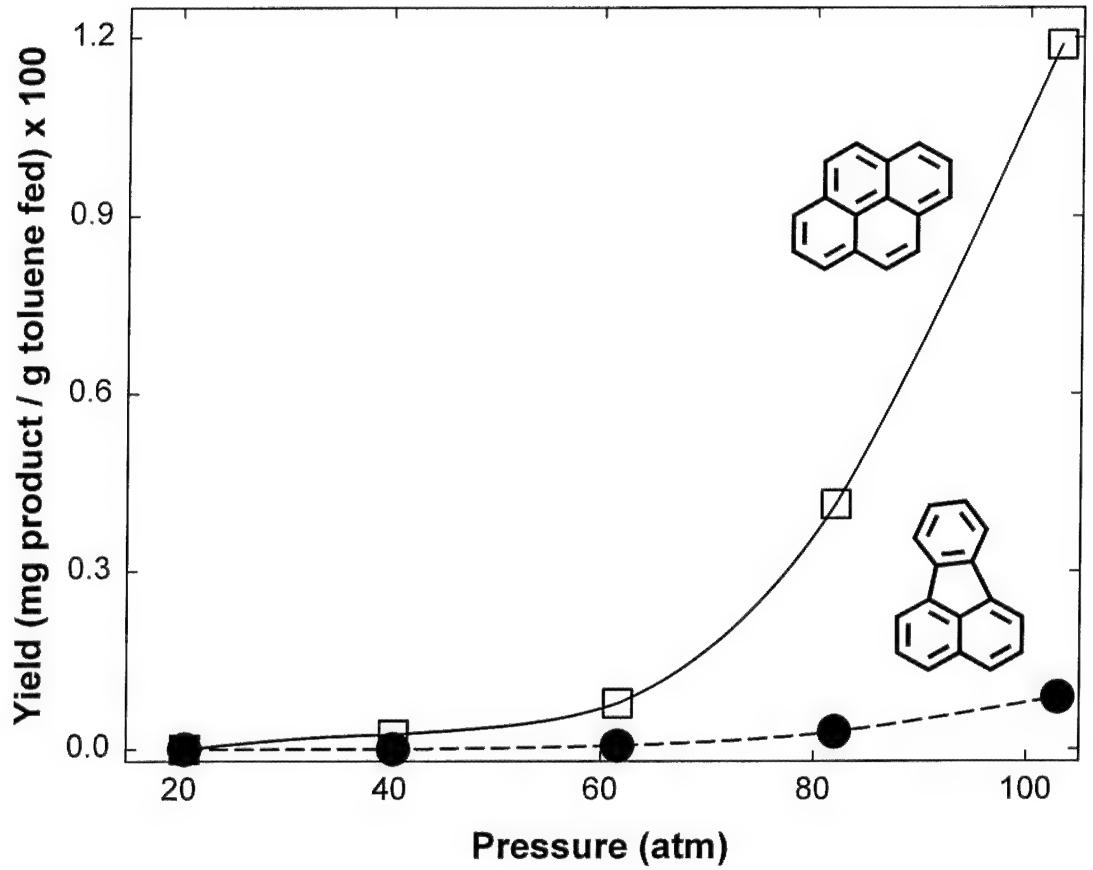


**Figure 16.** Yields of pyrene and fluoranthene, as functions of pressure, from toluene pyrolysis at 535 °C and 550 sec.

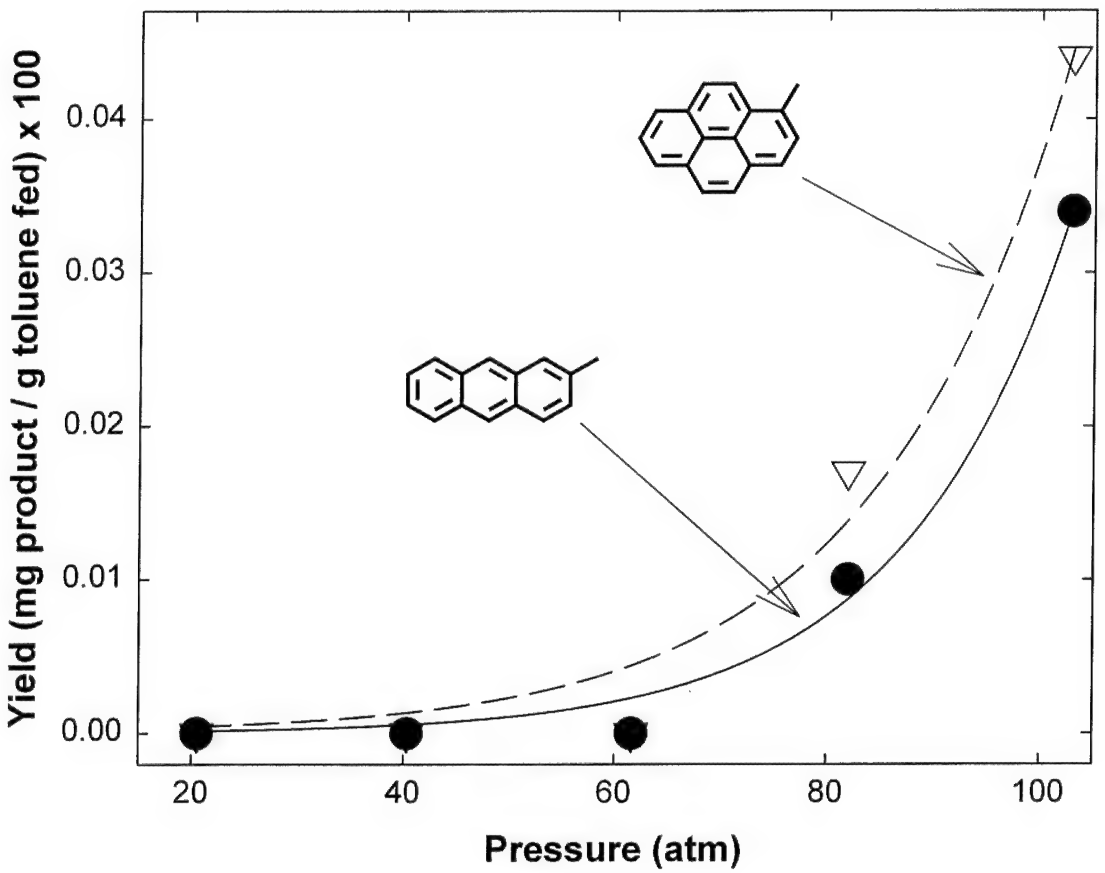


**Figure 17.** Yields of 2-methylanthracene and 1-methylpyrene, as functions of pressure, from toluene pyrolysis at 535 °C and 550 sec.

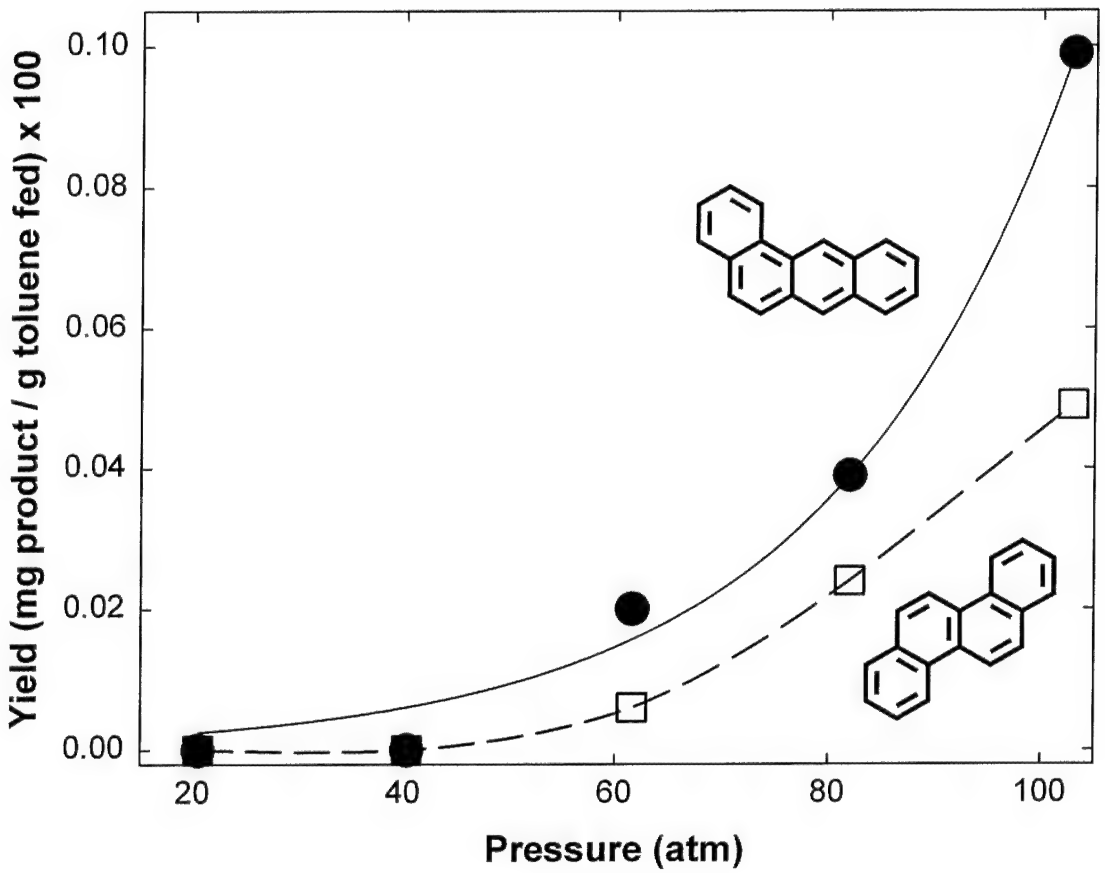


**Figure 18.** Yields of benz[*a*]anthracene and chrysene, as functions of pressure, from toluene pyrolysis at 535 °C and 550 sec.

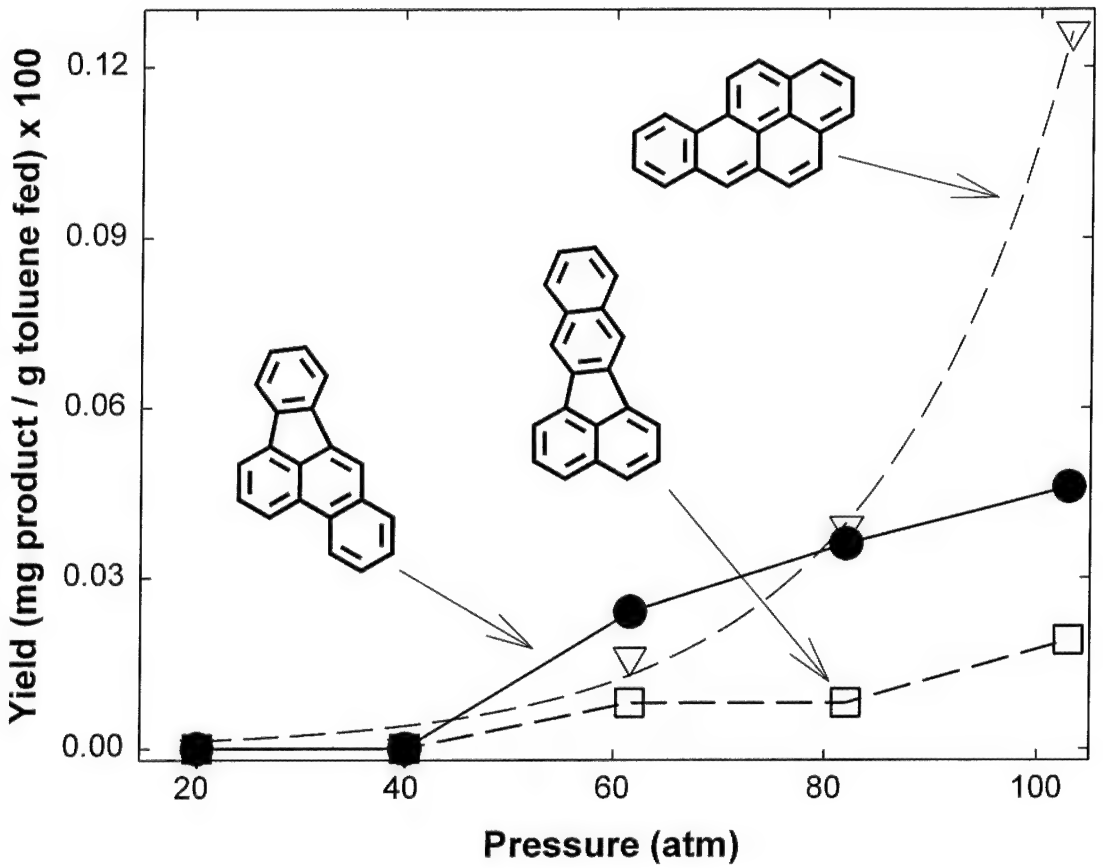


**Figure 19.** Yields of benzo[*a*]pyrene, benzo[*b*]fluoranthene and benzo[*k*]fluoranthene, as functions of pressure, from toluene pyrolysis at 535 °C and 550 sec.

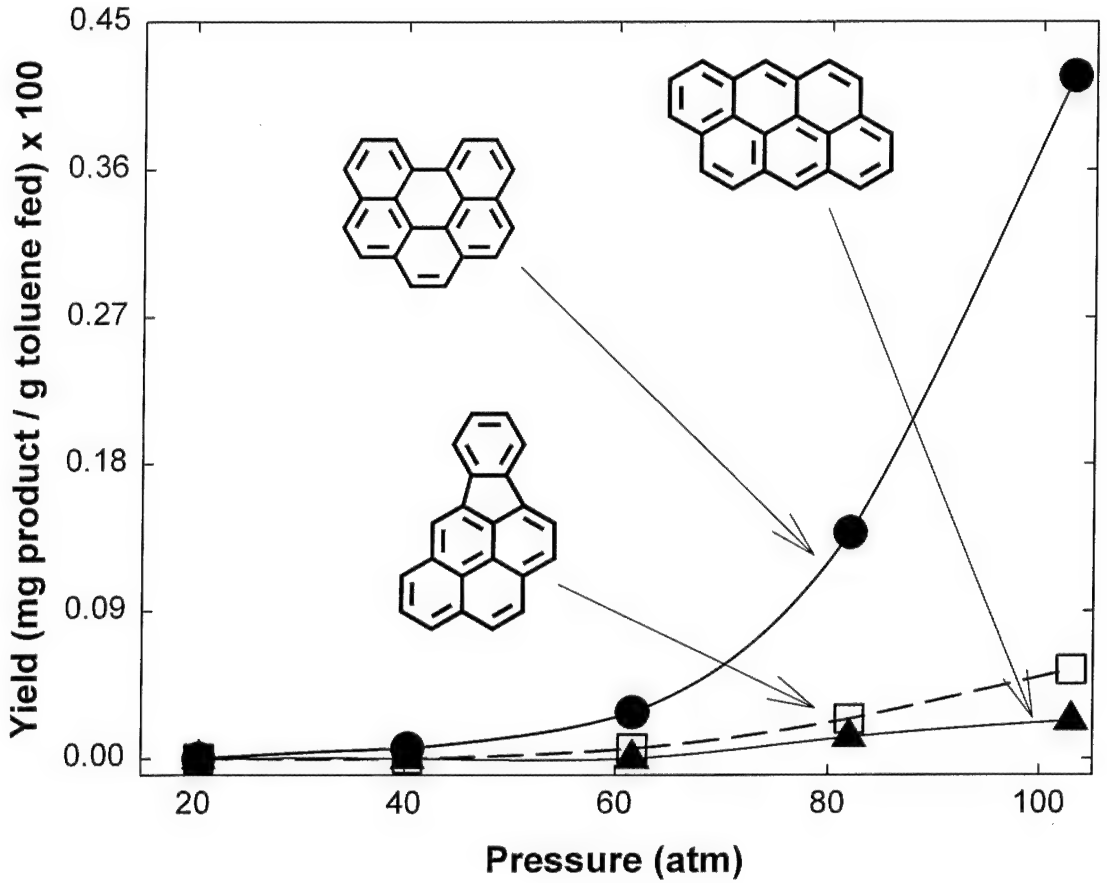


**Figure 20.** Yields of indeno[1,2,3-*cd*]pyrene, benzo[*ghi*]perylene and anthanthrene, as functions of pressure, from toluene pyrolysis at 535 °C and 550 sec.

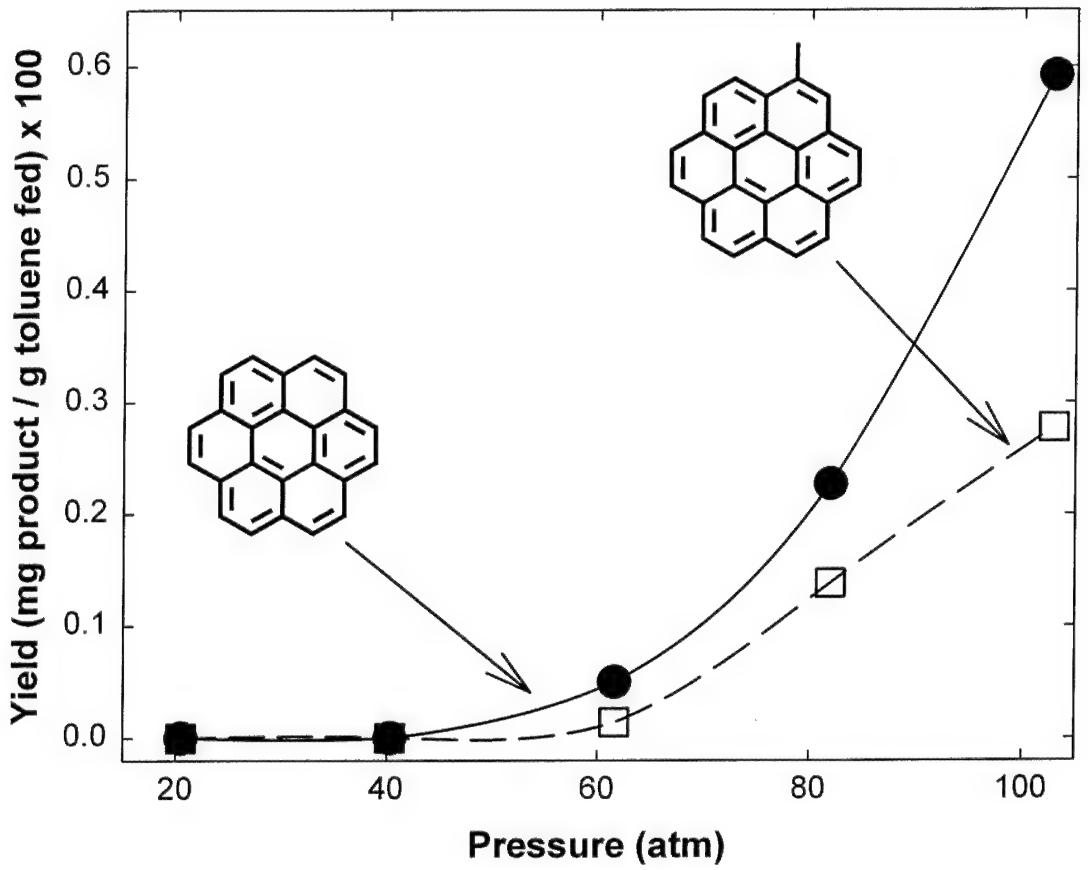


**Figure 21.** Yields of coronene and 1-methylcoronene, as functions of pressure, from toluene pyrolysis at 535 °C and 550 sec.

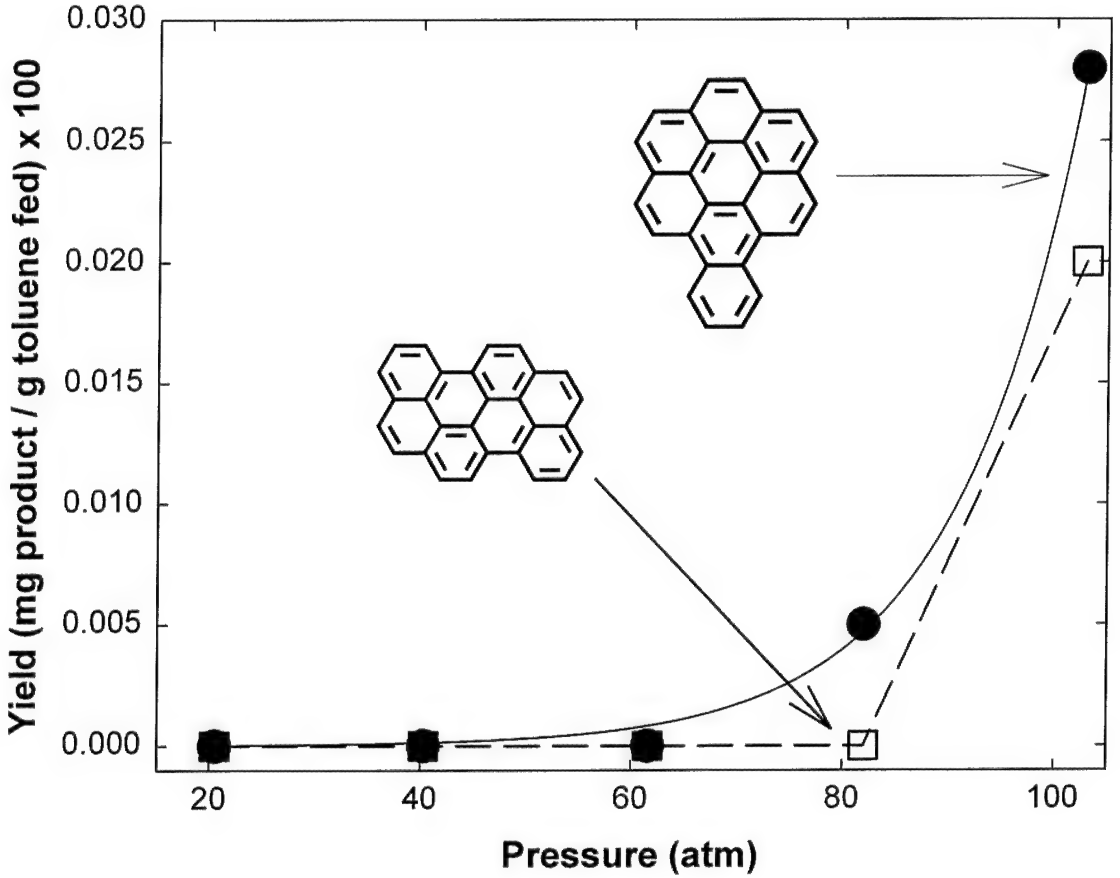


**Figure 22.** Yields of benzo[*a*]coronene and benzo[*pqr*]naphtho[8,1,2-*bcd*]perylene, as functions of pressure, from toluene pyrolysis at 535 °C and 550 sec.

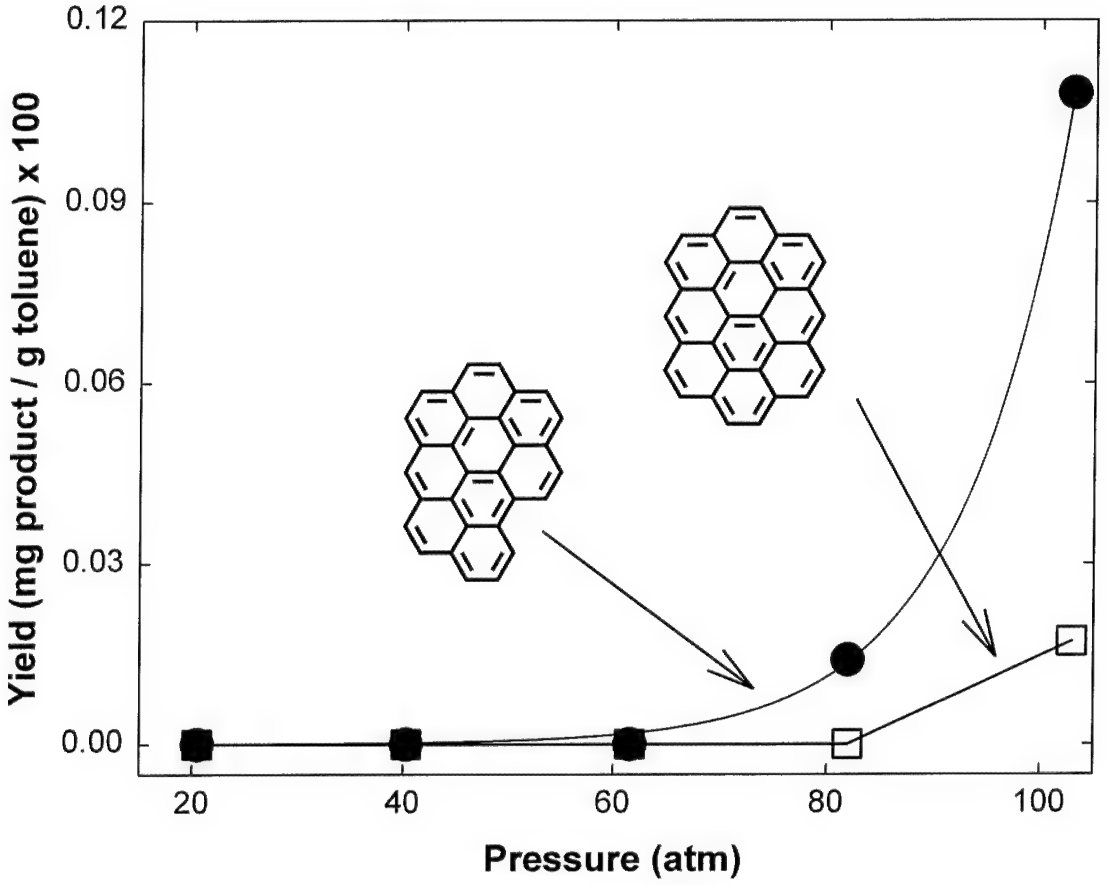


**Figure 23.** Yields of naphtho[8,1,2-*abc*]coronene and ovalene, as functions of pressure, from toluene pyrolysis at 535 °C and 550 sec.

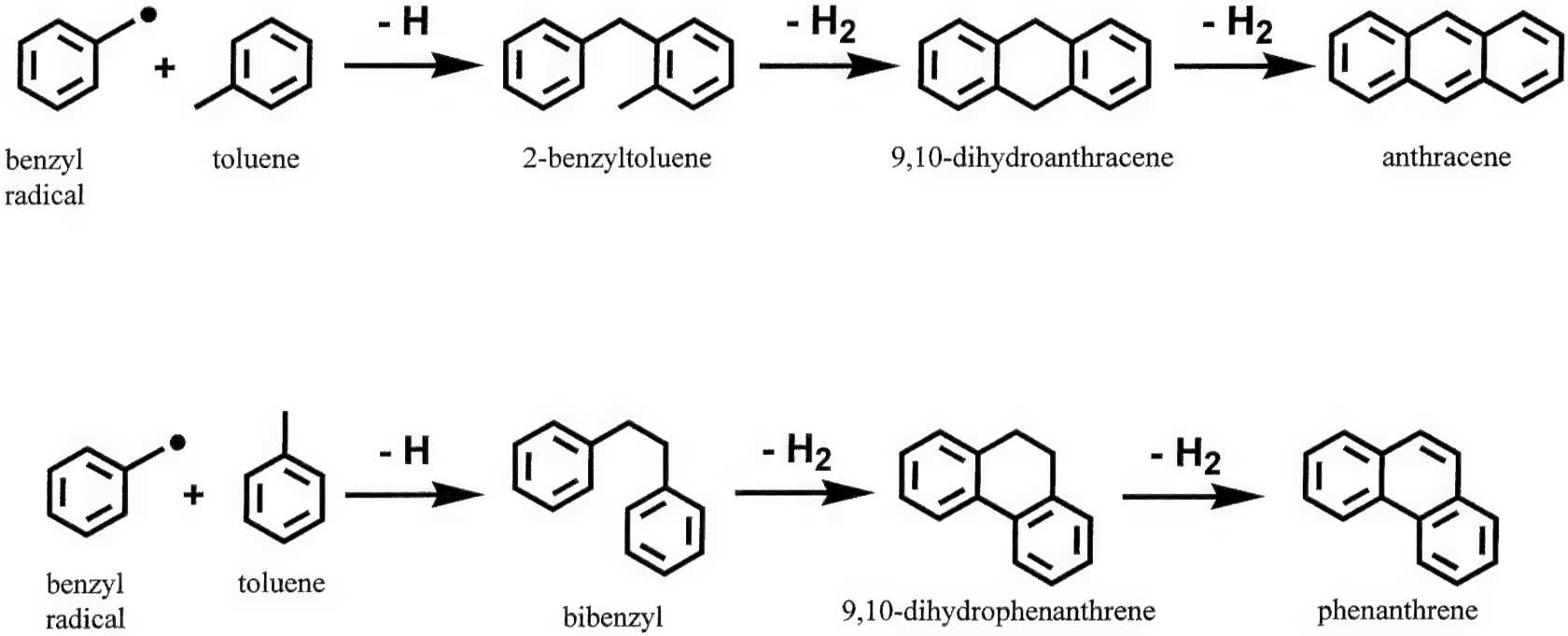


**Figure 24.** Proposed schemes for $C_{14}H_{10}$ PAH formation at high pressures. Adapted and extended from Colket and Seery, 1994.

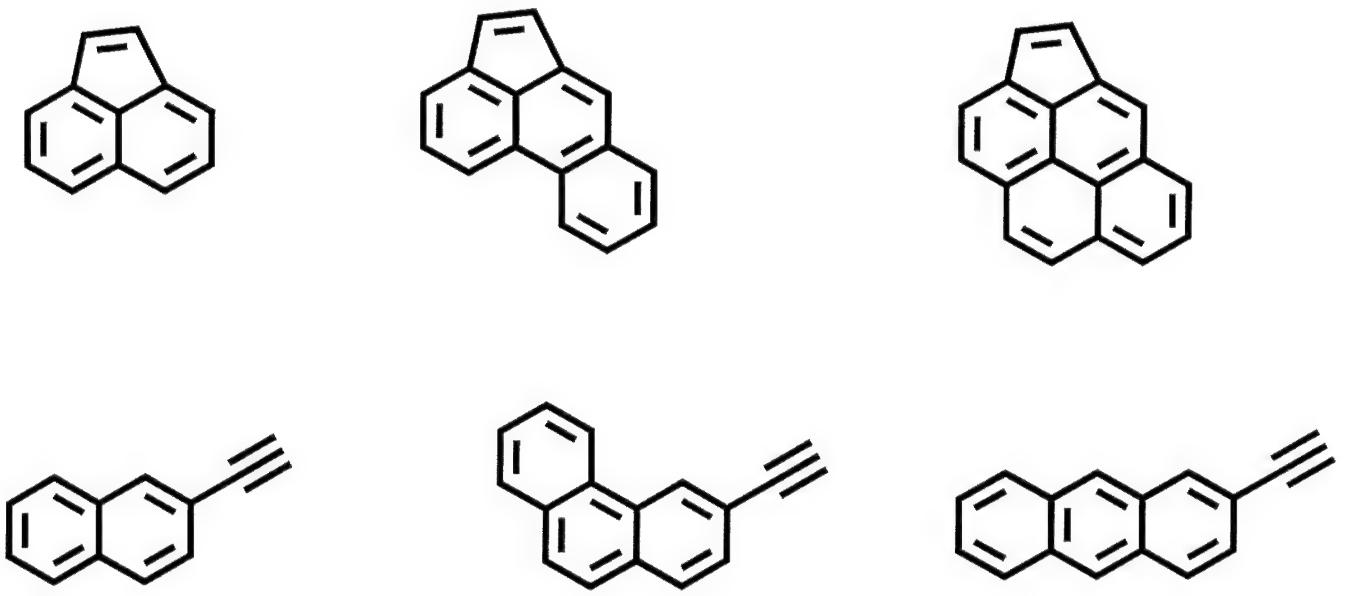

**Figure 25.** Two classes of PAH not observed in the supercritical toluene pyrolysis experiments, cyclopenta-fused PAH (top row) and ethynyl-substituted PAH (bottom row).

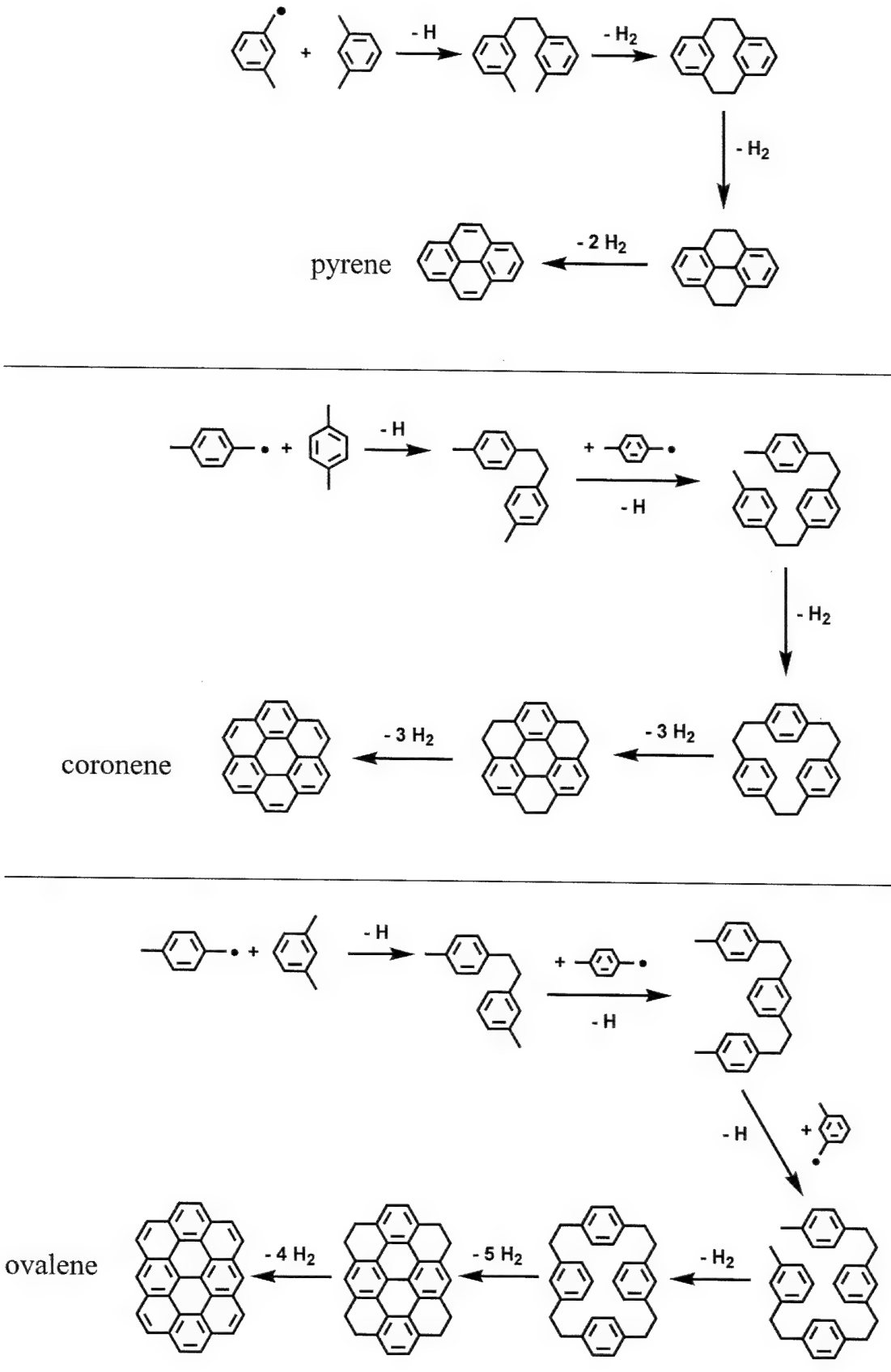


**Figure 26.** Postulated schemes for the formation of pyrene, coronene, and ovalene from xylenes and their radicals.

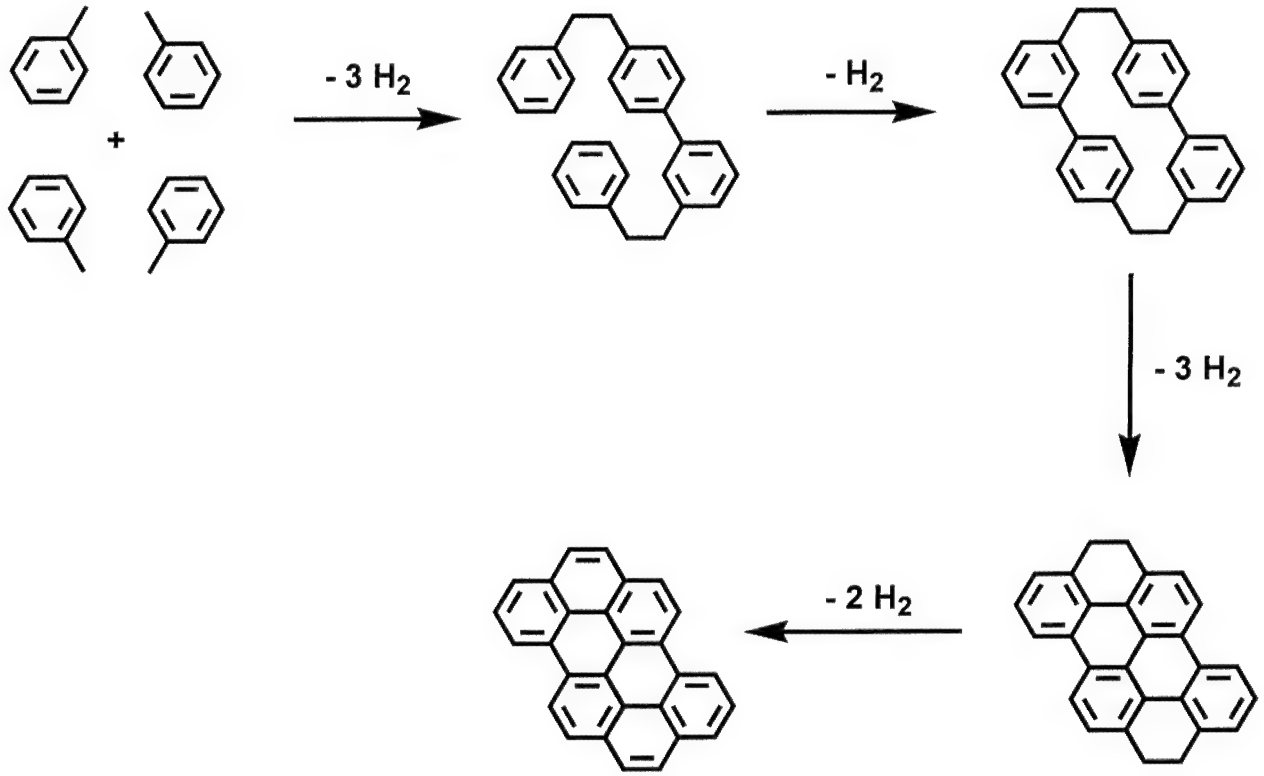


benzo[*pqr*]naphtho[8,1,2-*bcd*]perylene

**Figure 27.** Postulated reaction mechanism for the formation of benzo[*pqr*]naphtho[8,1,2-*bcd*]perylene from supercritical pyrolysis of toluene.

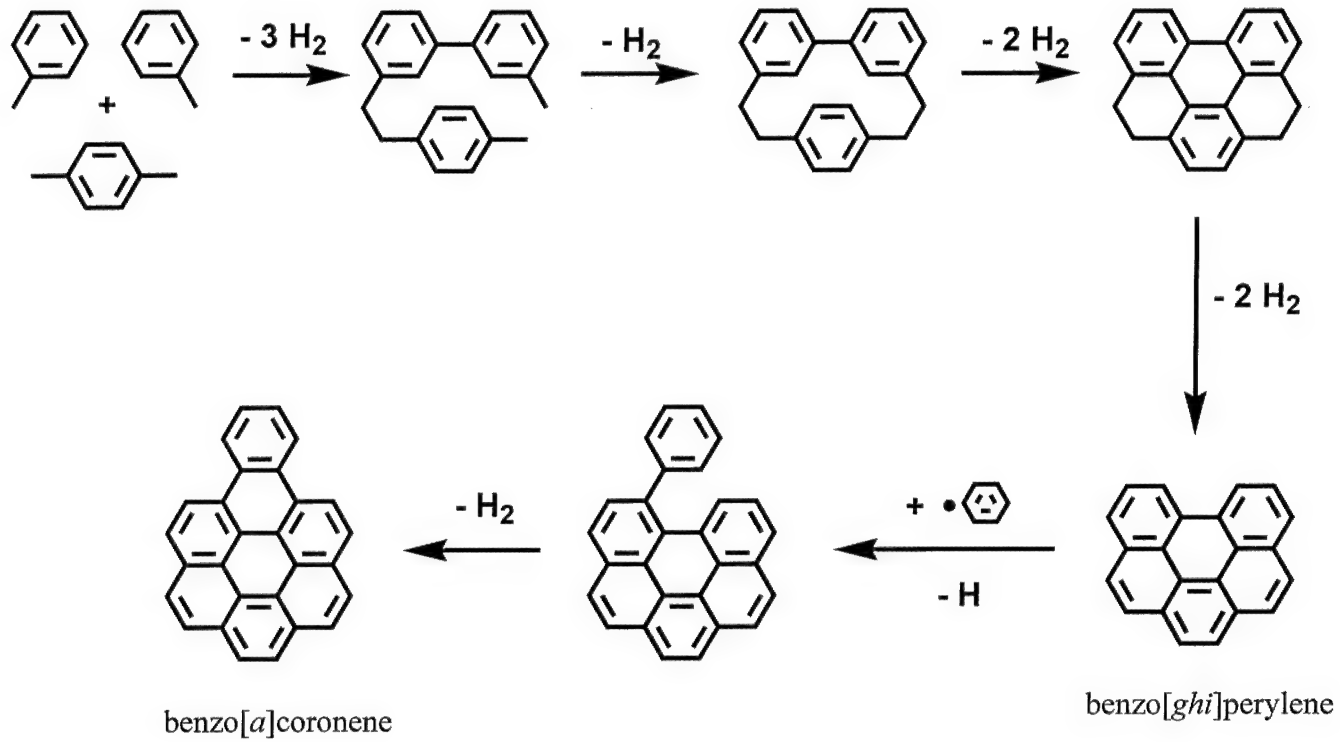


**Figure 28.** Postulated reaction mechanism for the formation of benzo[*ghi*]perylene and benzo[*a*]coronene from supercritical pyrolysis of toluene.

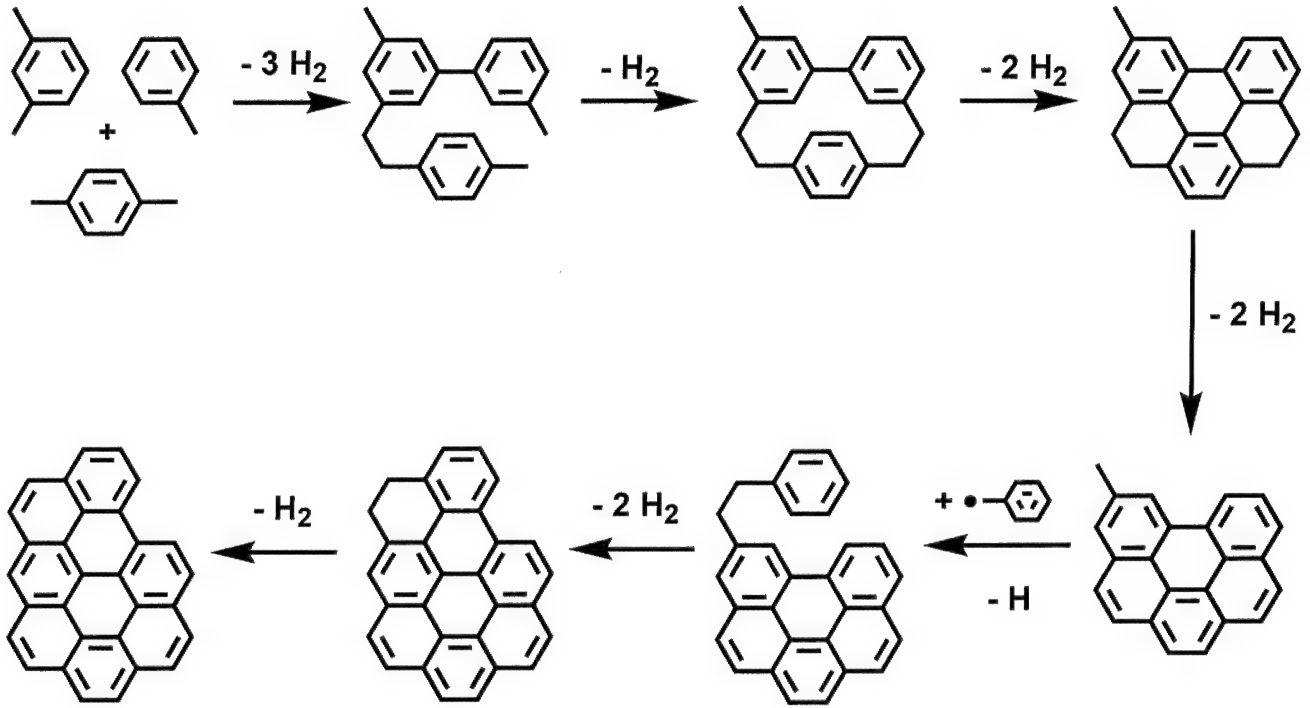


naphtho[*8,1,2-abc*]coronene

**Figure 29.** Postulated reaction mechanism for the formation of naphtho[8,1,2-*abc*]coronene from supercritical pyrolysis of toluene.

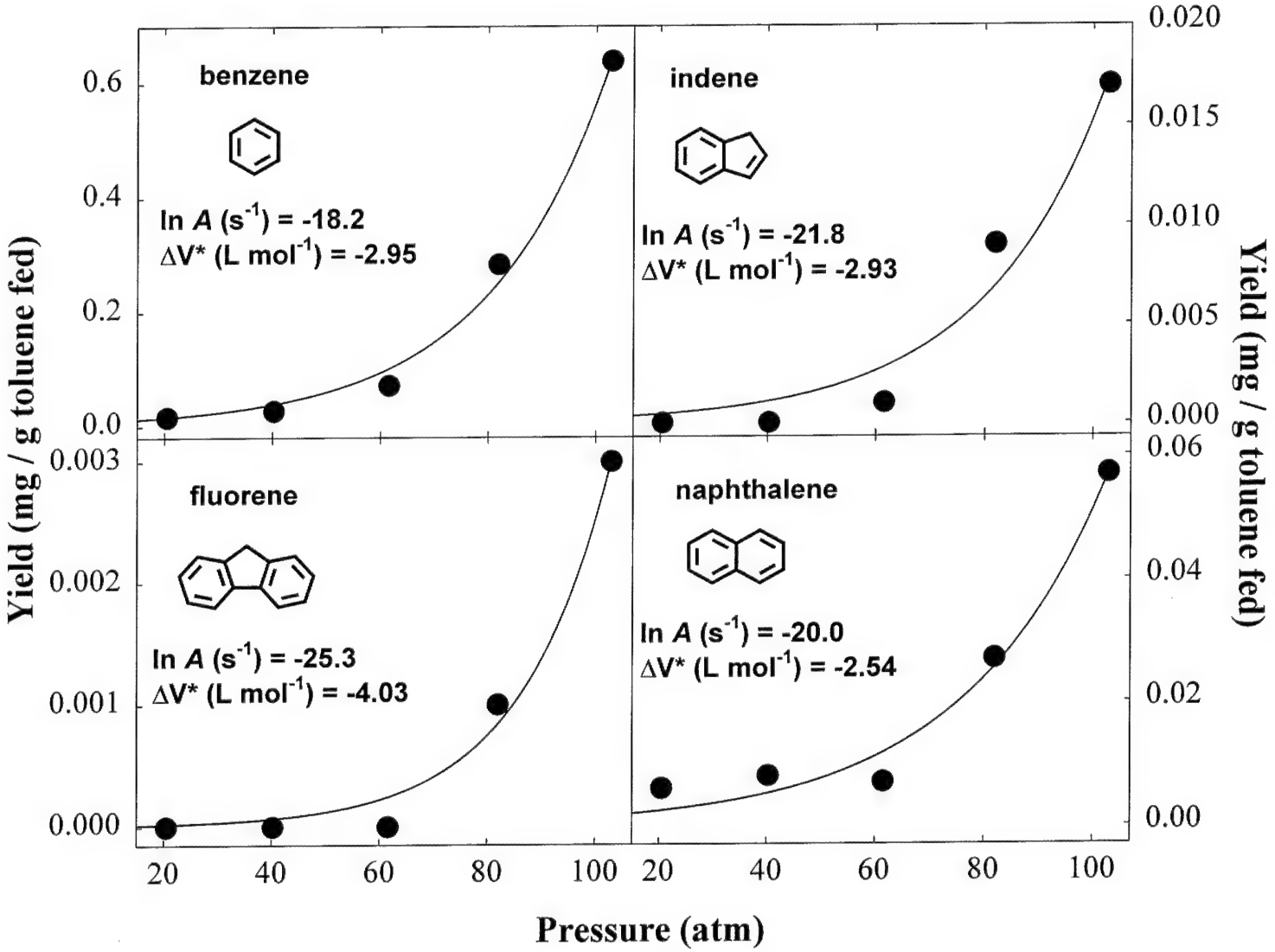


**Figure 30.** PAH yields, as functions of pressure, from toluene pyrolysis at 535 °C and 550 sec. Filled circles are experimental measurements. Curves are first-order global kinetics fits to the data, generated from Equation (5) in the text, and the values of ln *A* and ΔV* shown above for each product species.

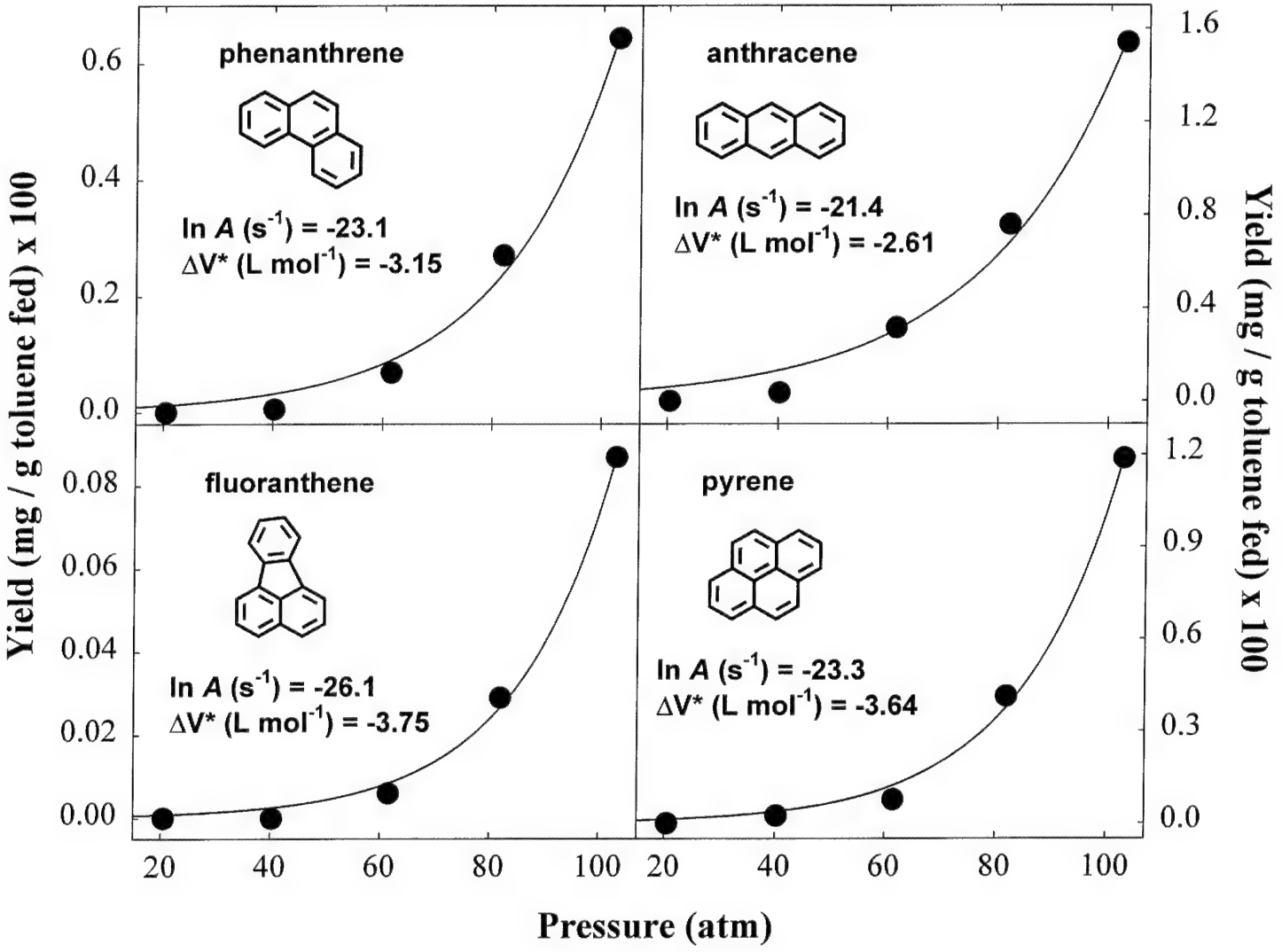


**Figure 31.** PAH yields, as functions of pressure, from toluene pyrolysis at 535 °C and 550 sec. Filled circles are experimental measurements. Curves are first-order global kinetics fits to the data, generated from Equation (5) in the text, and the values of ln *A* and ΔV* shown above for each product species.

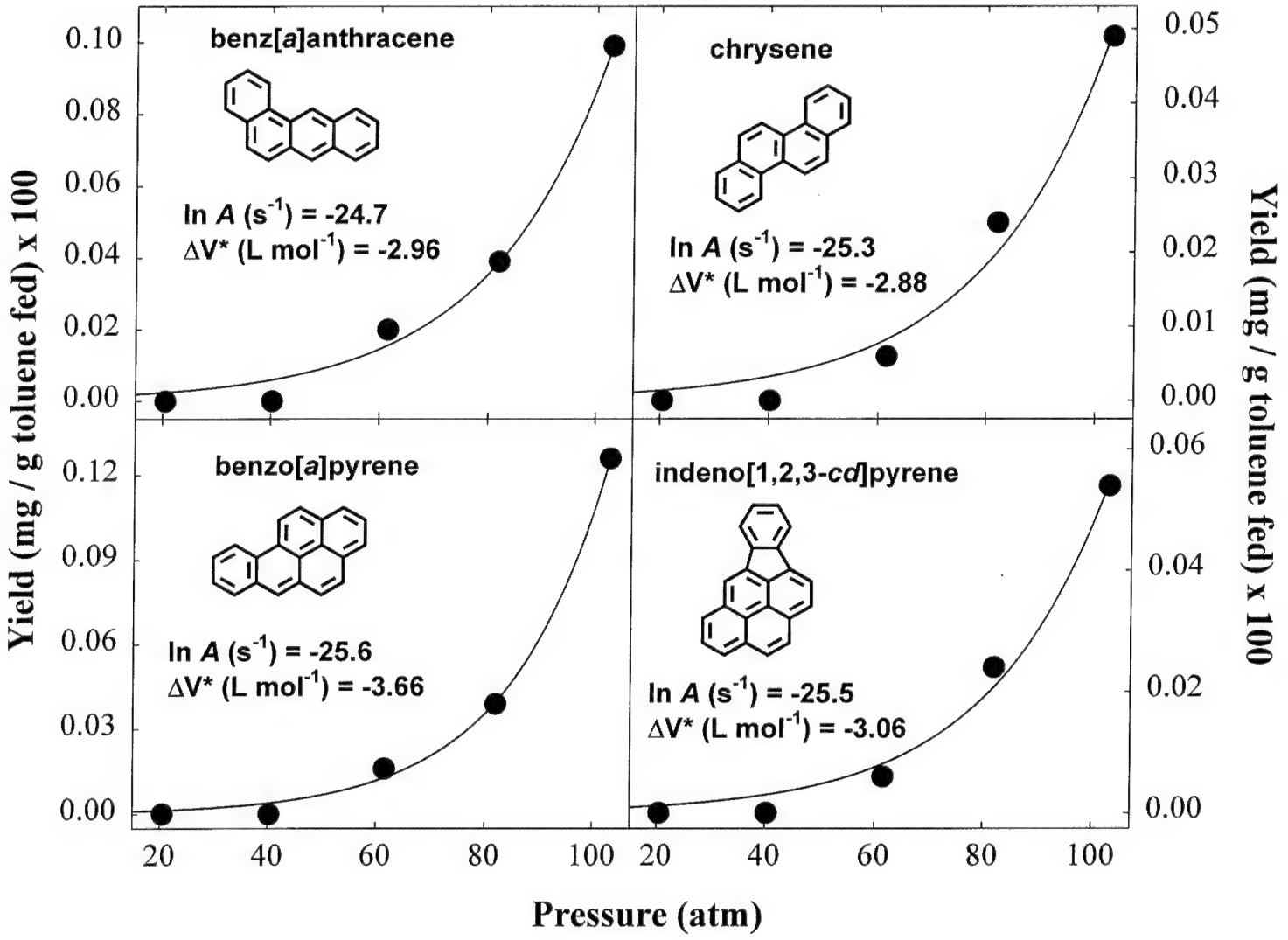


**Figure 32.** PAH yields, as functions of pressure, from toluene pyrolysis at 535 °C and 550 sec. Filled circles are experimental measurements. Curves are first-order global kinetics fits to the data, generated from Equation (5) in the text, and the values of ln *A* and ΔV* shown above for each product species.

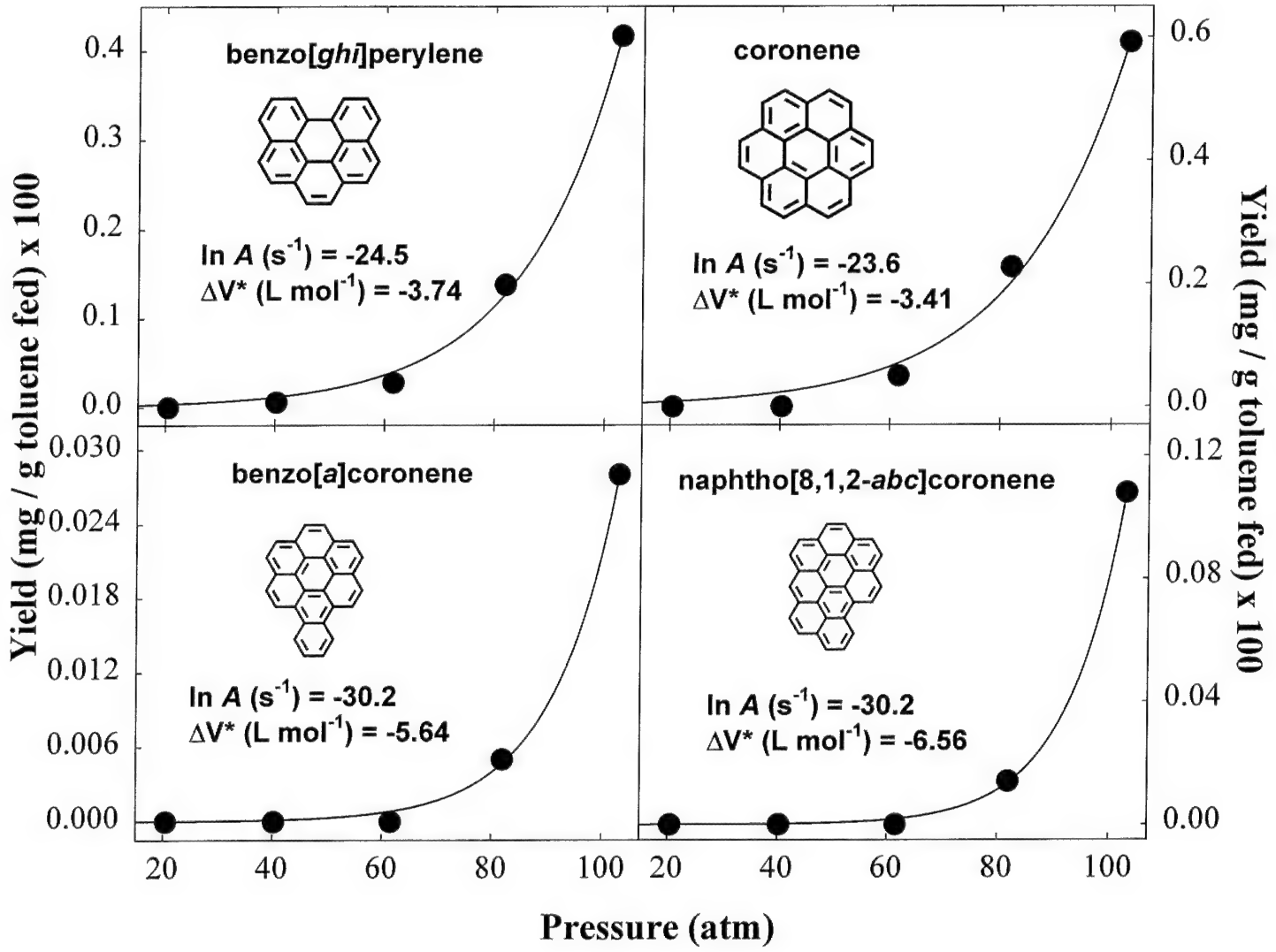


**Figure 33.** PAH yields, as functions of pressure, from toluene pyrolysis at 535 °C and 550 sec. Filled circles are experimental measurements. Curves are first-order global kinetics fits to the data, generated from Equation (5) in the text, and the values of ln *A* and ΔV* shown above for each product species.

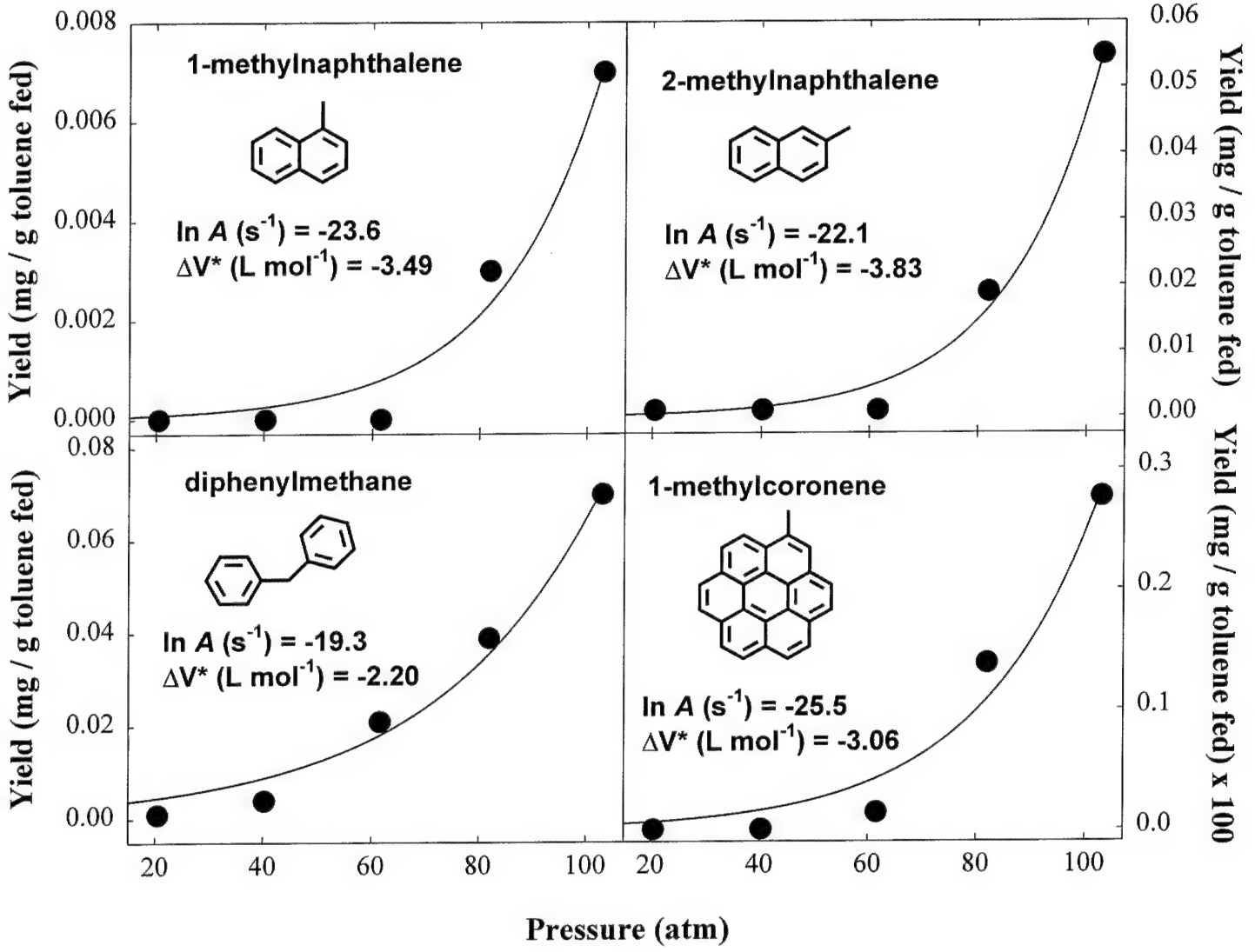


**Figure 34.** PAH yields, as functions of pressure, from toluene pyrolysis at 535 °C and 550 sec. Filled circles are experimental measurements. Curves are first-order global kinetics fits to the data, generated from Equation (5) in the text, and the values of ln *A* and ΔV* shown above for each product species.

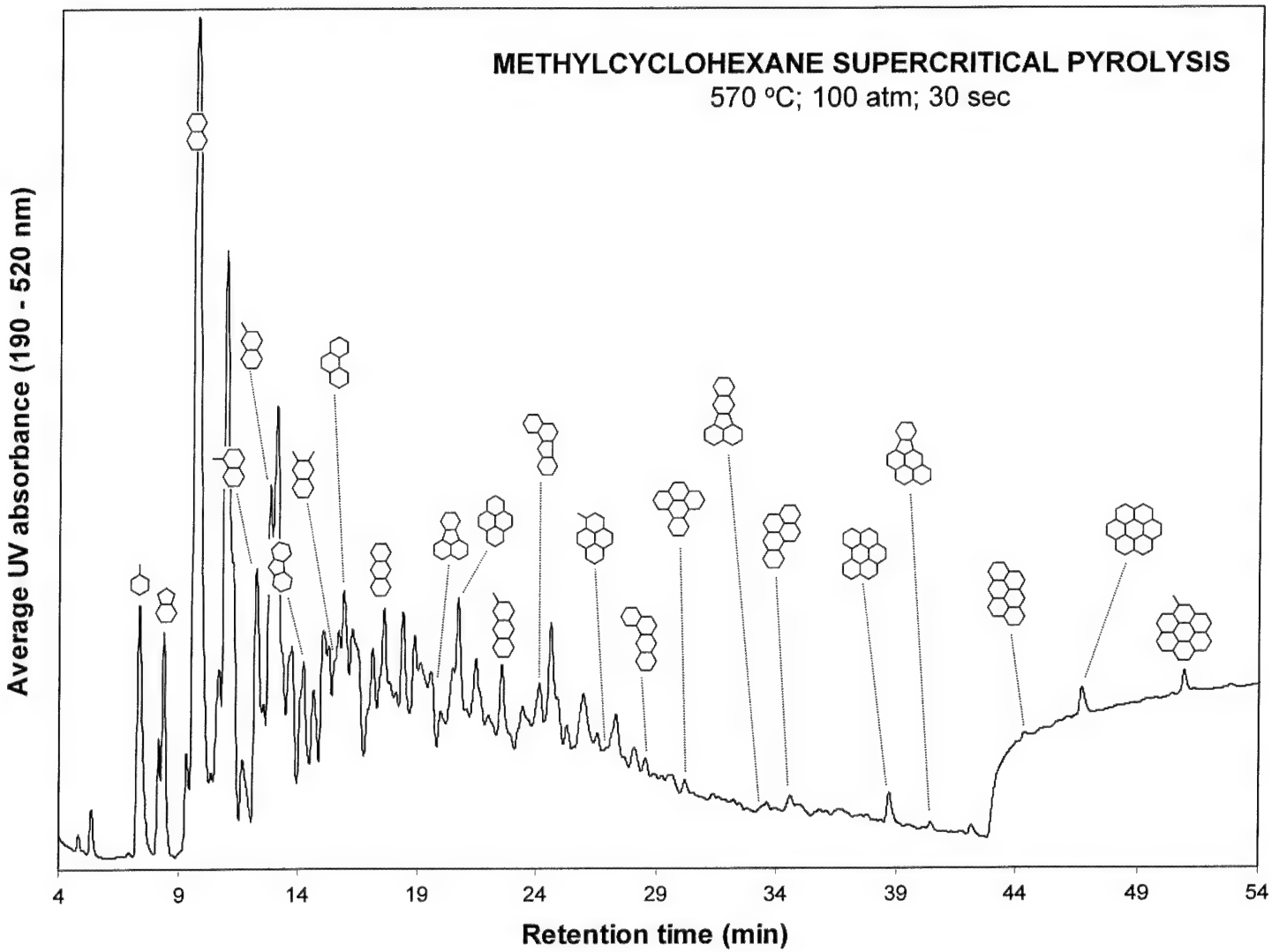


**Figure 35.** HPLC chromatogram of products of supercritical methylcyclohexane pyrolysis at 570 °C and 100 atm. Rise in baseline at ~ 43 minutes is due to a change in the HPLC mobile phase to the UV-absorbing dichloromethane. Identified components, from left to right, are: toluene, indene, naphthalene, 1-methylnaphthalene, 2-methylnaphthalene, fluorene, 2,3-dimethylnaphthalene, phenanthrene, anthracene, fluoranthene, pyrene, 2-methylanthracene, benzo[*a*]fluorene, 1-methylpyrene, benz[*a*]anthracene, benzo[*e*]pyrene, benzo[*k*]fluoranthene, benzo[*a*]pyrene, benzo[*ghi*]perylene, indeno[1,2,3-*cd*]pyrene, anthanthrene, coronene, 1-methylcoronene.

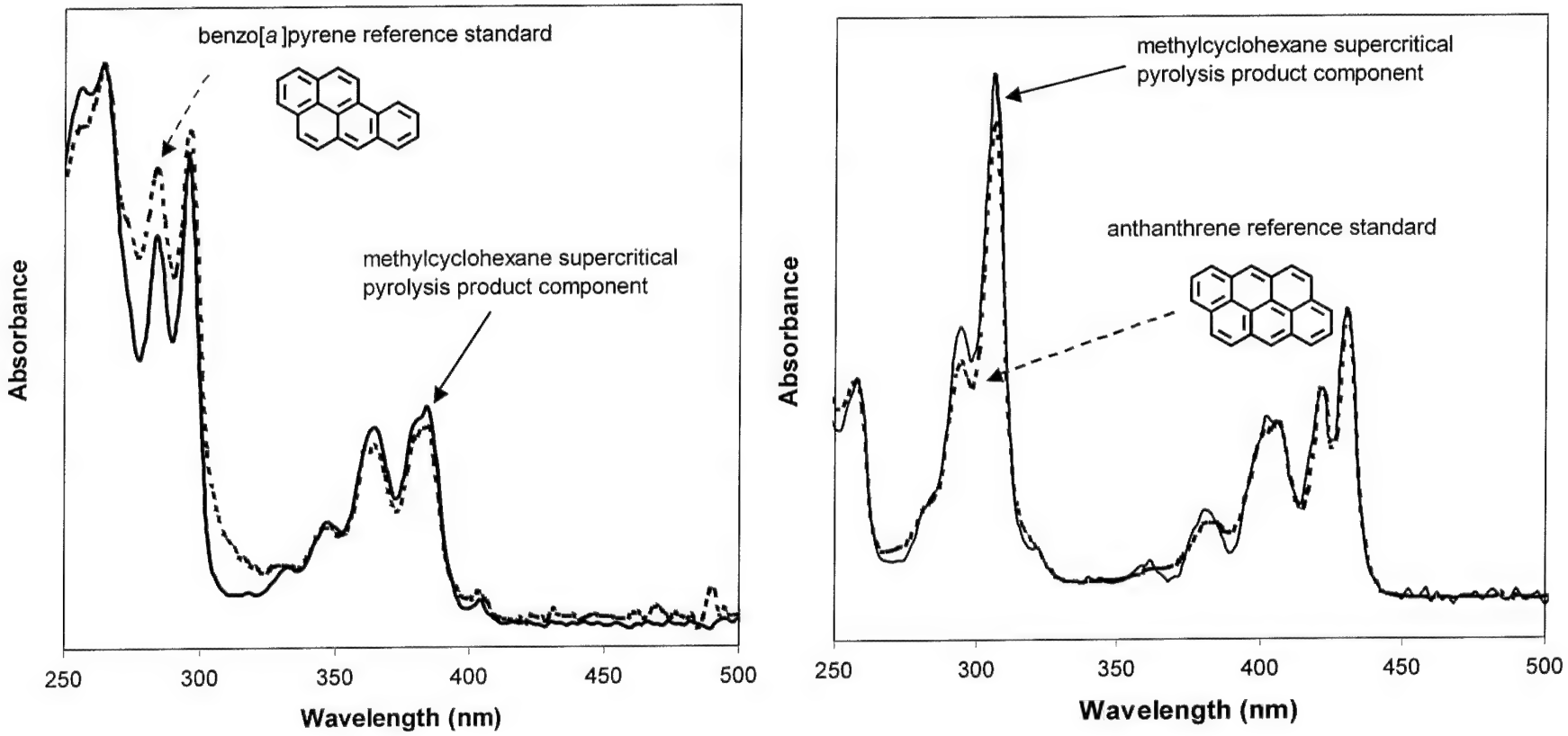


**Figure 36.** Matching UV absorption spectra of reference standards (dashed lines) and methylcyclohexane pyrolysis product components (solid lines): benzo[*a*]pyrene and anthanthrene.

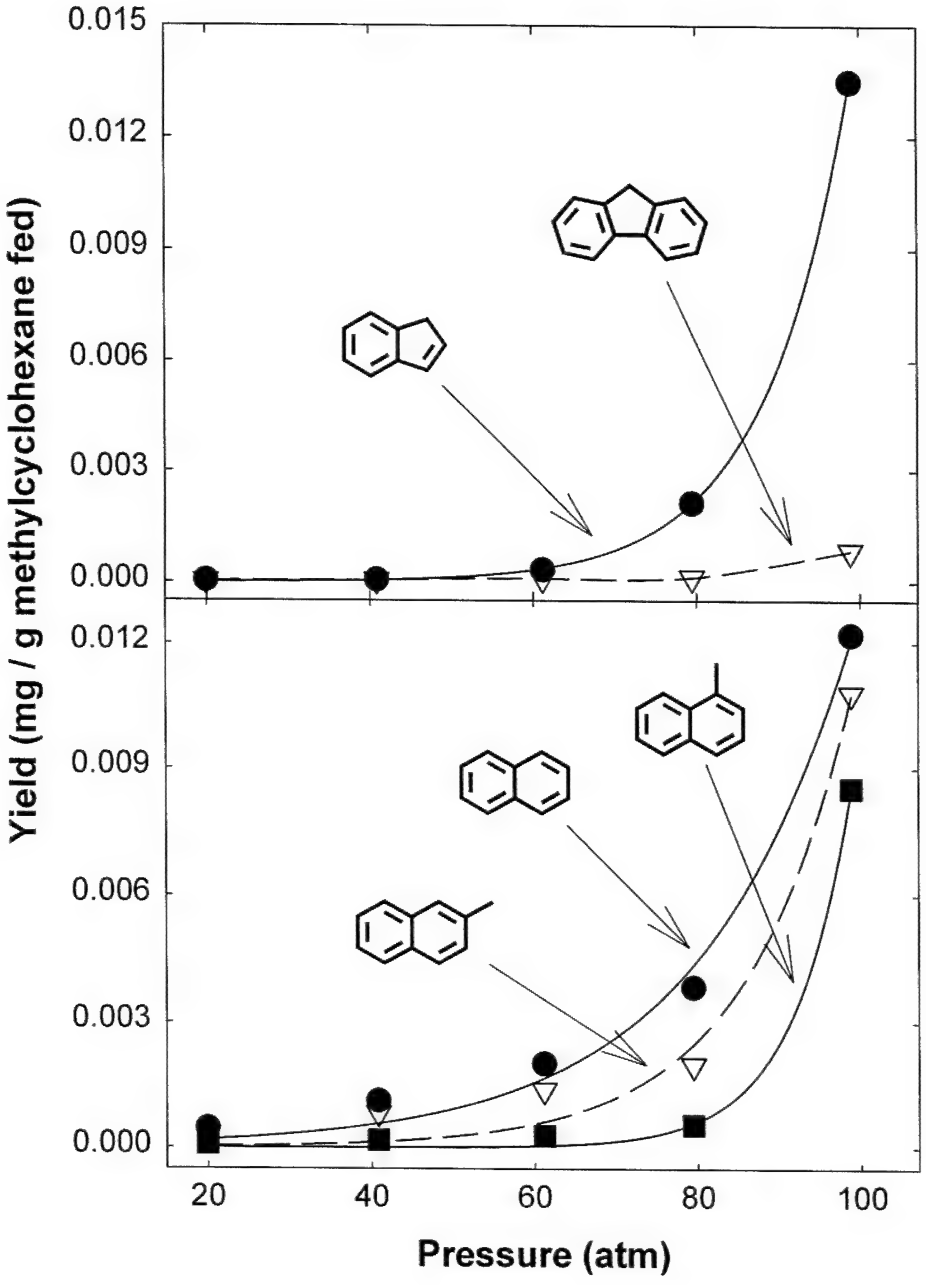


**Figure 37.** Yields of 2- and 3-ring PAH, as functions of pressure, from methylcyclohexane pyrolysis at 570 $^{o}$C and 30 sec.

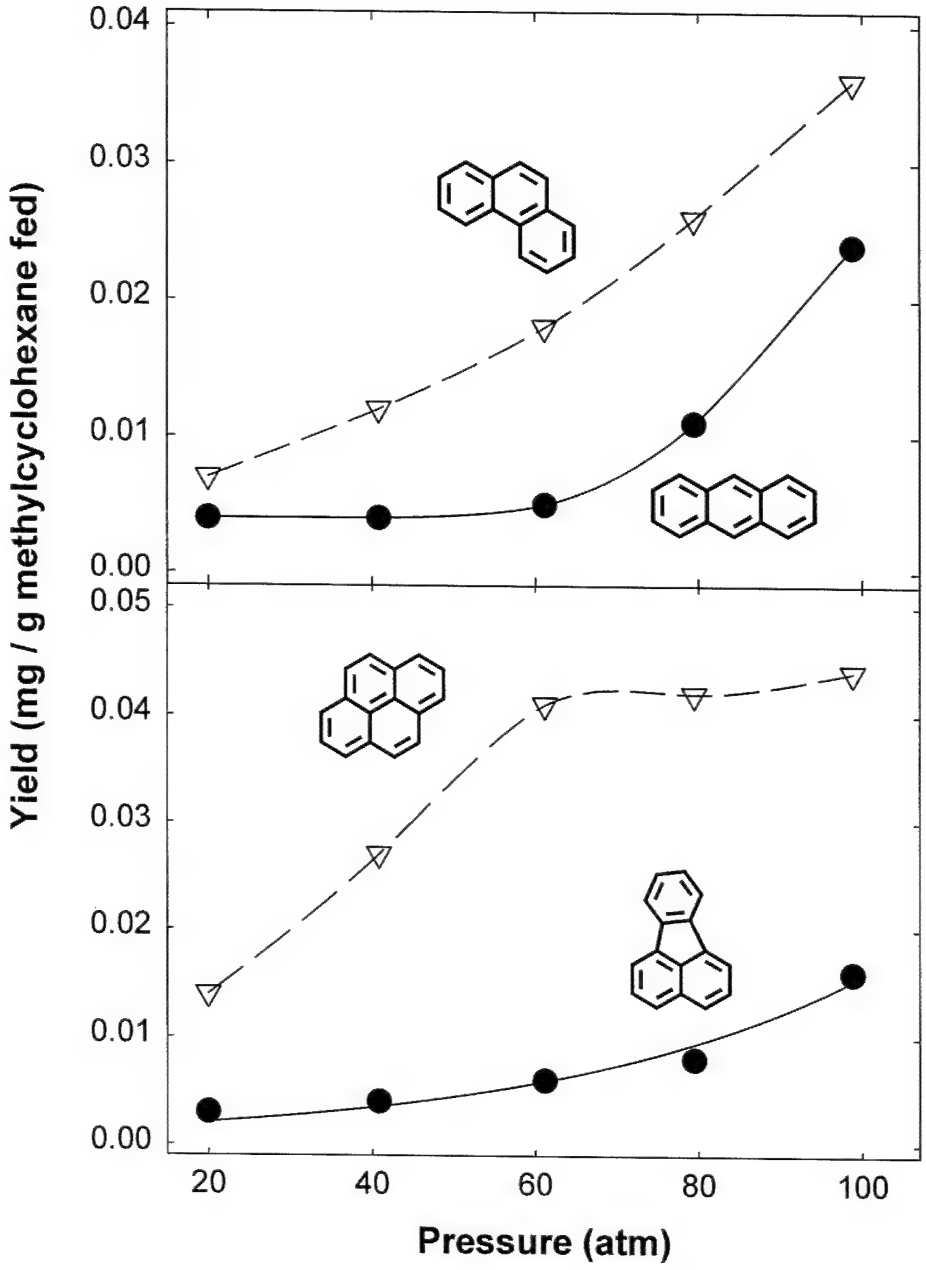


**Figure 38.** Yields of 3- and 4-ring PAH, as functions of pressure, from methylcyclohexane pyrolysis at 570 °C and 30 sec.

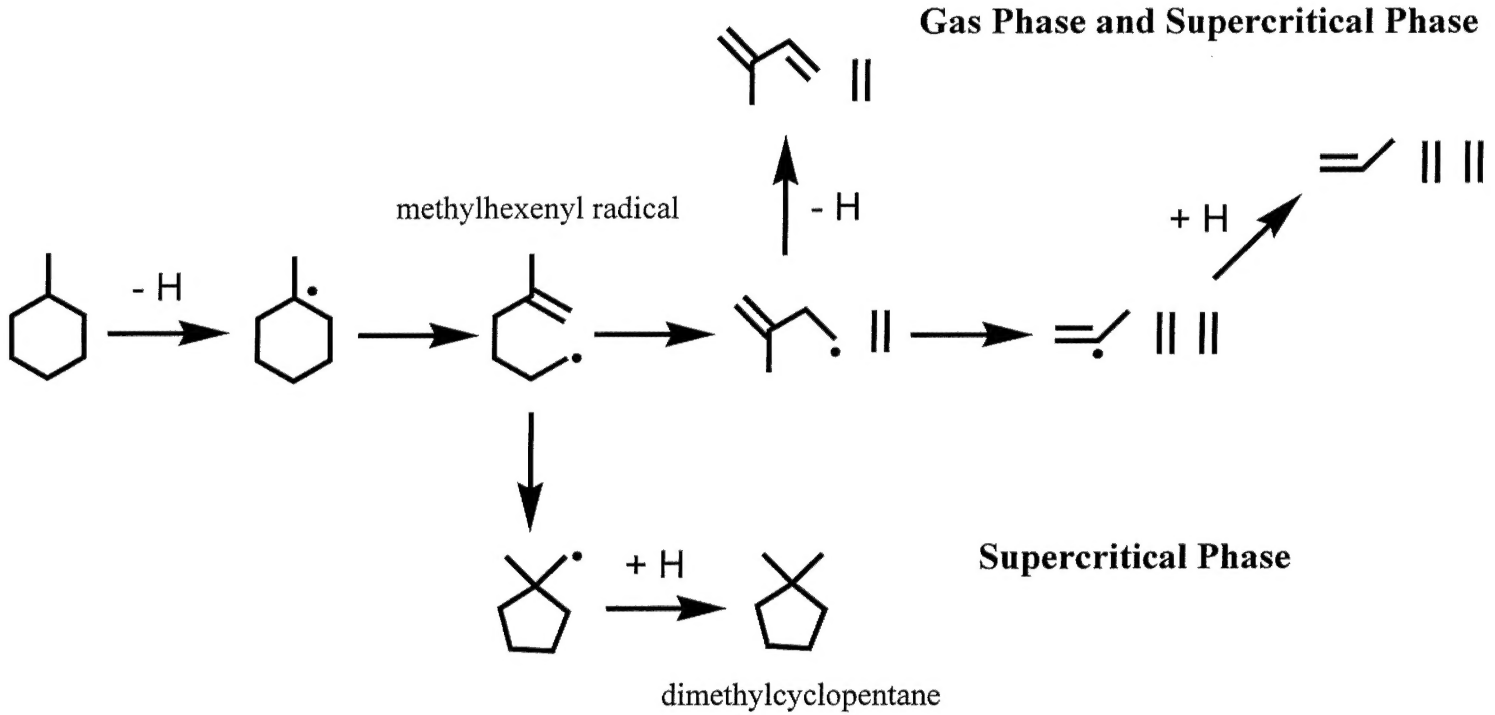


**Figure 39.** Dimethylcyclopentane produced from supercritical methylcyclohexane pyrolysis. Adapted from Stewart [Stewart, 1999].

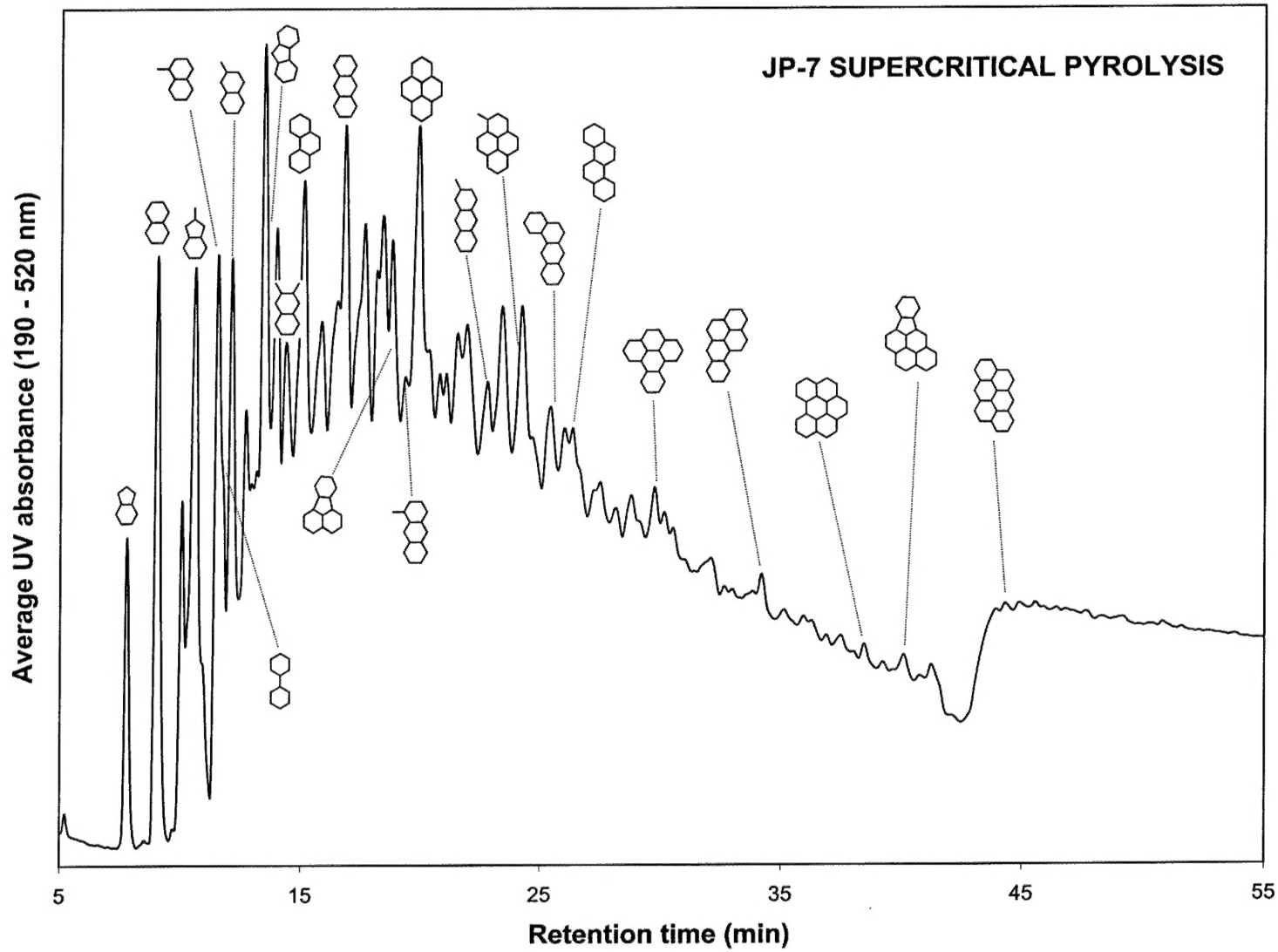


**Figure 40.** HPLC chromatogram of products of supercritical JP-7 pyrolysis. JP-7 fuel sample provided by Dr. H. Huang, United Technologies Research Center. Rise in baseline at ~ 43 minutes is due to a change in the HPLC mobile phase to the UV-absorbing dichloromethane. Identified components, from left to right, are: indene, naphthalene, 2-methylindene, 1-methylnaphthalene, biphenyl, 2-methylnaphthalene, fluorene, 2,3-dimethylnaphthalene, phenanthrene, anthracene, fluoranthene, 1-methylanthracene, pyrene, 2-methylanthracene, 1-methylpyrene, benz[*a*]anthracene, chrysene, benzo[*e*]pyrene, benzo[*a*]pyrene, benzo[*ghi*]perylene, indeno[1,2,3-*cd*]pyrene, and anthanthrene.

**Principal Investigator Annual Data Collection (PIADC) Survey Form**

NOTE: If there is insufficient space on this survey to meet your data submissions, please submit additional data in the same format as identified below.

PI DATA

Name (Last, First, MI): Wornat, Mary J.

Institution Princeton University

Contract/Grant No. F49620-00-1-0298

NUMBER OF CONTRACT/GRANT CO-INVESTIGATORS

Faculty__1__ Post Doctorates__1____ Graduate Students___1___ Other____2___

PUBLICATIONS RELATED TO AFOREMENTIONED CONTRACT/GRANT

NOTE: List names in the following format: Last Name, First Name, MI

Include: Articles in peer reviewed publications, journals, book chapters, and editorships of books.

Do Not Include: Unreviewed proceedings and reports, abstracts, "Scientific American" type articles, or articles that are not primary reports of new data, and articles submitted or accepted for publication, but with a publication date outside the stated time frame.

Name of Journal, Book, etc.:

Title of Article:

Author(s):

Publisher (if applicable):

Volume:_____ Page(s):_____ Month Published:_____ Year published:_____

## HONORS/AWARDS RECEIVED DURING CONTRACT/GRANT LIFETIME

Include: All honors and awards received during the lifetime of the contract or grant, and any life achievement honors such as (Nobel prize, honorary doctorates, and society fellowships) prior to this contract or grant.

Do Not Include: Honors and awards unrelated to the scientific field covered by the contract/grant.

Honor/Award:_____ Year Received:_____

Honor/Award Recipient(s):_____

Awarding Organization:_____